Spin-orbit coupling in periodic systems with broken time-reversal symmetry: Formal and computational aspects

Spin-Orbit Coupling in Time Reversal Symmetry Broken Periodic Systems: Formal and Computational Aspects

Jacques K. Desmarais,[1,2,3,*] Jean-Pierre Flament,[4] and Alessandro Erba[1,†]

[1] *Dipartimento di Chimica, Università di Torino, via Giuria 5, 10125 Torino, Italy*
[2] *Department of Geological Sciences, University of Saskatchewan, Saskatoon, SK S7N 5E2, Canada*
[3] *Department of Physics and Engineering Physics, University of Saskatchewan, Saskatoon, SK S7N 5E2, Canada*
[4] *Université de Lille, CNRS, UMR 8523 — PhLAM — Physique des Lasers, Atomes et Molécules, 59000 Lille, France*

(Dated: June 3, 2020)

We discuss the treatment of spin-orbit coupling (SOC) in time reversal symmetry broken periodic systems for relativistic electronic structure calculations of materials within the generalized non-collinear Kohn-Sham density functional theory (GKS-DFT). We treat SOC self-consistently and express the GKS orbitals in a two-component spinor basis. Crucially, we present a methodology (and its corresponding implementation) for the simultaneous self-consistent treatment of SOC and exact non-local Fock exchange operators. The many advantages of the inclusion of non-local Fock exchange in the self-consistent treatment of SOC, as practically done in hybrid exchange-correlation functionals, are both formally derived and illustrated through numerical examples: i) it imparts a local magnetic torque (i.e. the ability of the two-electron potential to locally rotate the magnetization with respect to a starting guess configuration) that is key to converge to the right solution in non-collinear DFT regardless of the initial guess for the magnetization; ii) because of the local magnetic torque, it improves the rotational invariance of non-collinear formulations of the DFT; iii) it introduces the dependence on specific pieces of the spinors (i.e. those mapped onto otherwise missing spin-blocks of the complex density matrix) into the two-electron potential, which are key to the correct description of the orbital- and spin-current densities and their coupling with the magnetization; iv) when space-inversion symmetry is broken, it allows for the full breaking of time-reversal symmetry in momentum space, which would otherwise be constrained by a sum-rule linking the electronic band structure at opposite points in the Brillouin zone ($\underline{\mathbf{k}}$ and -$\underline{\mathbf{k}}$). The presented methodology is implemented in a developmental version of the public CRYSTAL code. Numerical tests are performed on the model system of an infinite radical chain of Ge_2H with both space-inversion and time-reversal symmetries broken, which allows to highlight all the above-mentioned effects.

Keywords:

I. INTRODUCTION

Symmetry breaking is of fundamental interest to condensed matter physics as it leads to the advent of many phenomena in materials, particularly so for magnetic systems. For example, the breaking of space inversion symmetry is a prerequisite for the appearance of piezoelectricity, optical activity in chiral materials,[1] and for the Dzyaloshinskii-Moriya effect, which plays a central role in the creation of magnetic skyrmions.[2] Moreover, the breaking of time-reversal symmetry is required for the appearance of the magneto-optical effect,[1] and the anomalous Hall effect.[3]

In the broad field of spintronics, in which electronic devices are devised by manipulating the charge and spin degrees of freedom, the most interesting materials are those in which both space inversion and time-reversal symmetries are simultaneously broken.[4] On the one hand, the breaking of time-reversal symmetry possibly leads to a sizable spin current available for manipulation. On the other hand, the breaking of space inversion symmetry has significant consequences in the presence of a strong spin-orbit coupling (SOC). In such a fully relativistic picture, the breaking of space inversion symmetry indeed results in the creation of an effective internal magnetic field through the Rashba spin-orbit interaction (in 2D materials) or the Dresselhaus spin-orbit interaction (in bulk 3D crystals),[5,6] which play a key role in the appearance of non-trivial topological states of matter, such as topological insulators, Weyl semimetals, magnetic hopfions and Majorana fermions, as well as the related quantum spin-Hall effect.[3,4,7,8] As a consequence, there is great interest in the possibility of developing accurate formal and computational schemes capable of describing time-reversal symmetry broken periodic systems within a fully relativistic framework.

Although the treatment of time-reversal symmetry broken (TRSB) systems can be achieved in a formally well defined way from wavefunction-based methods, using for example the most general four-component theory of Dirac (or also two-component variants), the corresponding methodologies can hardly be applied to materials of interest.[9–11] Practical calculations in computational materials science are typically performed within the density functional theory (DFT) instead. However, explicit relativistic exchange-correlation functionals for TRSB systems (with a dependence on the particle-number density n, the magnetization vector $\underline{\mathbf{m}} = [m_x, m_y, m_z]$, as well as the SOC-induced orbital-current

density vector $\underline{\mathbf{j}} = [j_x, j_y, j_z]$, and the three spin-current density vectors $\underline{\mathbf{J}}_x = [J_{xx}, J_{xy}, J_{xz}]$, $\underline{\mathbf{J}}_y = [J_{yx}, J_{yy}, J_{yz}]$, $\underline{\mathbf{J}}_z = [J_{zx}, J_{zy}, J_{zz}]$) are still to be devised.[12–17,46] In practice, relativistic calculations are usually performed with the so-called collinear or non-collinear formulations of the DFT, where use is made of standard non-relativistic functionals modified to only include the explicit dependence on n and m_z (collinear) or n and $\underline{\mathbf{m}}$ (non-collinear).[9,16,18–30] In this paper we analyze some of the limitations due to the lack of such explicit relativistic functionals for calculations on TRSB materials and we present a strategy to overcome most of them.

Our interest here is the density functional treatment of TRSB materials in the absence of external magnetic and electric fields. However, it is worth acknowledging important formal advancements within the so-called spin-current-DFT (SCDFT):[31] a theoretical framework initially formulated for treating external fields in a scalar-relativistic context that was then generalized to the description of SOC.[32] In the presence of an external magnetic field with an arbitrary direction, the exchange-correlation functional approximations within the SCDFT should depend explicitly on the particle-number density n, the magnetization vector $\underline{\mathbf{m}}$, the field-induced orbital-current density vector $\underline{\mathbf{j}}$ and on the three spin-current density vectors $\underline{\mathbf{J}}_x$, $\underline{\mathbf{J}}_y$ and $\underline{\mathbf{J}}_z$.[31] In this context (i.e. scalar-relativistic description in the presence of external fields), exchange-correlation functionals that also include a dependence on the field-induced $\underline{\mathbf{j}}$ have been devised for treating TRSB systems and tested for such purposes.[33–40] Let us stress that, while these functionals have been developed and used for calculations with external fields, their practical ability to perform equally well on fully relativistic calculations remains an unanswered and interesting research topic. Elsewhere, a scheme has been proposed to generalize existing standard meta generalized gradient approximation (meta-GGA) functionals to also include $\underline{\mathbf{j}}$ for finite field scalar-relativistic calculations.[41] This approach performs a simple substitution of the dependence of the functional on the kinetic-energy density τ to an expression involving the scalar product of $\underline{\mathbf{j}}$ with itself. However, such an approach poses a few major challenges to be overcome before its practical use will be possible to run actual relativistic calculations on TRSB systems and also does not provide a means to include the $\underline{\mathbf{J}}_x$, $\underline{\mathbf{J}}_y$ and $\underline{\mathbf{J}}_z$. The root of such challenges stem from the need for simultaneously treating also the non-collinear magnetization $\underline{\mathbf{m}}$ using these same meta-GGA functionals. Indeed, the treatment of non-collinear magnetization in functionals beyond the simple local density approximation (LDA) involves significant numerical instability problems (mainly related to the evaluation of gradients of the magnetization at points in space of small magnetization), which are now well documented in the literature.[16,21,22,24,42,43] Furthermore, we have recently shown that even for the simpler GGA functionals, existing non-collinear formulations were not even rotationally invariant, because of the inconsistent use of signs of the different components of the magnetization in the expression of the exchange-correlation potential.[16] It is also worth mentionning, that the non-collinear formulation of Scalmani and Frisch does not reproduce the dependence on the transverse spin gradients obtained non-empirically by Eich and co-workers from the spin-polarized homogeneous electron gas.[24,44,45] This means that the formulation and implementation of new non-collinear schemes for calculations involving a dependence of the functional on $\underline{\mathbf{m}}$, $\underline{\mathbf{j}}$ and the $\underline{\mathbf{J}}_c$ would be useful. Along these lines, an interesting research direction towards the simultaneous treatment of $\underline{\mathbf{m}}$, $\underline{\mathbf{j}}$ and the $\underline{\mathbf{J}}_c$ in functionals beyond the LDA is represented by the alternative substitution schemes for the (spin-)current and magnetization gradient variables theorized by Pittalis *et al.*.[46]

Bearing in mind the afore-mentioned difficulties, while the use of orbital-current density $\underline{\mathbf{j}}$ and spin-current density $\underline{\mathbf{J}}_c$ dependent functionals for fully-relativistic calculations on TRSB systems is an interesting future prospect, it is far from being common. As a matter of fact, most practical fully-relativistic DFT calculations are still performed with functionals that do not have a proper dependence on $\underline{\mathbf{j}}$ and the $\underline{\mathbf{J}}_c$, with consequences to be addressed in this paper.

We show that the consequence of the lack of explicit treatment of current-densities in standard KS-DFT calculations can result in unphysical distributions of both the magnetization $\underline{\mathbf{m}}$ and the current densities, and hence in a poor description of the electronic structure of the system when a SOC operator is included in the Hamiltonian. Moreover, we discuss how plain DFT functionals belonging to either the LDA or the GGA produce a two-electron potential that lacks in local magnetic torque (i.e. the ability of the two-electron potential to locally rotate the magnetization during the SCF procedure, with respect to a starting guess configuration).[16,48–50] We show how this can sometimes lead to the inability of KS-DFT calculations to converge to the right spatial distribution for the magnetization, and how it affects the rotational invariance of the theory. We note that such a local magnetic torque was first discussed in TRSB materials, also taking into account orbital currents in a previous study by Sharma and co-workers.[51] Furthermore, we derive a sum-rule for the electronic band structure in TRSB periodic systems, which shows that standard KS-DFT calculations are unable to fully break time-reversal symmetry in momentum space, and access the full range of possible TRSB states.

Finally, through a formal analysis and numerical tests we show that all of the afore-mentioned limitations of practical relativistic KS-DFT calculations can be resolved by including a fraction of exact non-local Fock exchange in the Hamiltonian, as done in so-called hybrid exchange-correlation functionals, thus providing with a simple practical recipe. In this light, we here present the first implementation of a code for self-consistently treating both SOC and non-local Fock exchange in periodic systems in a fully two-component relativistic framework.

Before closing the introduction we stress the following two points:

1. These benefits of an inclusion of non-local Fock exchange occur because of its self-consistent treatment along with SOC in a two-component spinor basis. This point implies that those benefits would not be achieved in a calculation where the Fock exchange operator were to be evaluated instead in a one-component basis, as would be the case, for example, using the popular second-variational approach to SOC of existing implementations.[52–57]

2. Such a treatment also allows to include the effects of electron correlation. This point represents a distinction with respect to the previous work by Trushin and Görling for treating Fock exchange in periodic systems from a local rather than non-local potential from the optimized effective potential method with the exact exchange functional (EXX-OEP) within the SCDFT.[11,51,58]

II. FORMAL ASPECTS

A. Theoretical Framework

The standard non- or scalar-relativistic (SR) approach for treating time-reversal symmetry broken electronic states (often referred to as open-shell electronic configurations) is based on the unrestricted Hartree-Fock (UHF) or unrestricted (G)KS-DFT approaches, which both involve solving a set of two uncoupled secular equations, one for the α spin:

$$\tilde{\mathbf{H}}^{\alpha}_{\{\underline{\mathbf{k}}\}}\mathbf{C}^{\alpha}_{\{\underline{\mathbf{k}}\}} = \mathbf{S}^{\alpha}_{\{\underline{\mathbf{k}}\}}\mathbf{C}^{\alpha}_{\{\underline{\mathbf{k}}\}}\mathbf{E}^{\alpha}_{\{\underline{\mathbf{k}}\}} \ , \tag{1a}$$

and one for the β spin:

$$\tilde{\mathbf{H}}^{\beta}_{\{\underline{\mathbf{k}}\}}\mathbf{C}^{\beta}_{\{\underline{\mathbf{k}}\}} = \mathbf{S}^{\beta}_{\{\underline{\mathbf{k}}\}}\mathbf{C}^{\beta}_{\{\underline{\mathbf{k}}\}}\mathbf{E}^{\beta}_{\{\underline{\mathbf{k}}\}} \ , \tag{1b}$$

where $\underline{\mathbf{k}}$ is a point in momentum space, $\tilde{\mathbf{H}}_{\{\underline{\mathbf{k}}\}}$ is the Hamiltonian matrix in momentum space, which is obtained as a Fourier transform of the matrix in position space (the symbol tilde labels the SR Hamiltonian to distinguish it from the fully relativistic one to be introduced below), $\mathbf{C}_{\{\underline{\mathbf{k}}\}}$ is the matrix of the eigenvectors defining the crystalline orbitals (COs), $\mathbf{S}_{\{\underline{\mathbf{k}}\}}$ is the overlap matrix and $\mathbf{E}_{\{\underline{\mathbf{k}}\}}$ is the diagonal matrix of energy levels at point $\underline{\mathbf{k}}$ in the band structure of the system. To fix the notation, here matrices denoted with an upper-case latin letter have size $n \times n$, where n is the number of basis functions, while bold-underlined quantities are Cartesian vectors with size 3×1. The scheme sketched above is referred to as a one-component (1c) approach.

The procedure for performing instead fully relativistic calculations which also include SOC contributions is rather different. Indeed the SOC operator is distinct from other operators because i) it is complex in position space, and ii) it couples α and β components of the wave-function, such that it is no longer possible to solve for pure α and β states. This leads to the need to represent the wavefunction in terms of two-component (2c) spinors $\mathbf{\Psi}_i(\underline{\mathbf{r}};\underline{\mathbf{k}})$, which are written as a linear combination of Bloch functions as:

$$\mathbf{\Psi}_i(\underline{\mathbf{r}};\underline{\mathbf{k}}) = \sum_{\mu} \left[c^{\alpha}_{\mu i\{\underline{\mathbf{k}}\}}\boldsymbol{\alpha} + c^{\beta}_{\mu i\{\underline{\mathbf{k}}\}}\boldsymbol{\beta} \right] \phi_{\mu}(\underline{\mathbf{r}};\underline{\mathbf{k}}) \ , \tag{2}$$

where the $c_{\mu i\{\underline{\mathbf{k}}\}}$ are the complex coefficients of the COs, and $\boldsymbol{\alpha}$ and $\boldsymbol{\beta}$ are the simultaneous eigenfunctions of the spin operators $\hat{\mathbf{S}}^2$ and $\hat{S}_z$, which form a complete basis in spin space:

$$\boldsymbol{\alpha} = \begin{pmatrix} 1 \\ 0 \end{pmatrix} \quad \text{and} \quad \boldsymbol{\beta} = \begin{pmatrix} 0 \\ 1 \end{pmatrix} \ . \tag{3}$$

In our approach, the Bloch functions are expressed in terms of atom-centered functions, according to the so-called linear-combination of atomic orbitals (LCAO) framework, as follows:

$$\phi_{\mu}(\underline{\mathbf{r}};\underline{\mathbf{k}}) = \frac{1}{\sqrt{\Omega_r}} \sum_{\underline{\mathbf{g}}} \chi_{\mu}(\underline{\mathbf{r}} - \underline{\mathbf{g}} - \underline{\mathbf{a}}_{\mu}) e^{i\underline{\mathbf{k}}\cdot\underline{\mathbf{g}}} \ , \tag{4}$$

where χ_{μ} is an AO, $\underline{\mathbf{a}}_{\mu}$ its position vector in the reference lattice cell, $\underline{\mathbf{g}}$ is a direct lattice vector and Ω_r is the volume of the reciprocal primitive cell (the so-called first Brillouin zone). Our approach has been implemented in a developmental version of the CRYSTAL17 code.[59] We adopt a Kramers-unrestricted protocol, where the AOs are expressed in terms of real-solid-spherical Gaussian-type functions (GTF) up to angular momentum $l = 4$.[60] Both SR and SOC operators are represented in terms of relativistic effective-core potentials (RECP). Indeed, the RECP can be conveniently written as a sum of a purely SR term (the so-called averaged relativistic effective potential, AREP) and a purely SOC term (the so-called spin-orbit effectif potential, SOREP).[16,48,61,62]

The electronic structure of time-reversal symmetry broken systems from such a two-component theoretical framework in the presence of a SOC operator can be determined by self-consistently solving the generalized Hartree-Fock (GHF) or (G)KS-DFT secular equations:[16,48]

$$\begin{bmatrix} \mathbf{H}^{\alpha\alpha}_{\{\underline{\mathbf{k}}\}} & \mathbf{H}^{\alpha\beta}_{\{\underline{\mathbf{k}}\}} \\ \mathbf{H}^{\beta\alpha}_{\{\underline{\mathbf{k}}\}} & \mathbf{H}^{\beta\beta}_{\{\underline{\mathbf{k}}\}} \end{bmatrix} \begin{bmatrix} \mathbf{c}^{\alpha}_{\{\underline{\mathbf{k}}\}} \\ \mathbf{c}^{\beta}_{\{\underline{\mathbf{k}}\}} \end{bmatrix} = \begin{bmatrix} \mathbf{S}^{\alpha\alpha}_{\{\underline{\mathbf{k}}\}} & \mathbf{0} \\ \mathbf{0} & \mathbf{S}^{\beta\beta}_{\{\underline{\mathbf{k}}\}} \end{bmatrix} \begin{bmatrix} \mathbf{c}^{\alpha}_{\{\underline{\mathbf{k}}\}} \\ \mathbf{c}^{\beta}_{\{\underline{\mathbf{k}}\}} \end{bmatrix} \boldsymbol{\epsilon}_{\{\underline{\mathbf{k}}\}} \ , \tag{5}$$

which, unlike Eq. (1) now couple α and β components, and where matrices denoted with lower-case latin letters have size $n\times2n$ and $\boldsymbol{\epsilon}_{\{\underline{\mathbf{k}}\}}$ is the diagonal matrix of energy levels, with a size of $2n \times 2n$.

As long as time-reversal symmetry is preserved, Eq. (5) can be solved in a formally well-defined way for both GHF and generalized DFT methods. This is also true for TRSB systems for GHF. On the other hand, the situation is more challenging for methods based on

the DFT. This is because the standard collinear formulation of unrestricted (G)KS-DFT[29] does not result in a rotationally invariant theory for TRSB systems, when a SOC operator is included in the Hamiltonian. The rotational invariance can be regained in the local-density and generalized-gradient approximations (LDA and GGA) using appropriate non-collinear formulations of the DFT.[16,20,24] More specific details on our implementation of the GHF and generalized collinear and non-collinear DFT methods have been presented elsewhere for molecular (i.e. non-periodic) systems.[16,48]

The aspects discussed above on the consequences of the presence of the SOC operator in the Hamiltonian, change the symmetry properties of all operators in both position and momentum spaces, as well as the manner in which they are transformed from one space to another. In the following, we illustrate the properties of all operators in position and momentum space that are relevant to the self-consistent treatment of SOC for TRSB systems.

1. Matrix Elements in Position Space

We adopt a compact notation for the representation of matrix elements of operators in the direct lattice in the basis of AOs, as follows:

$$\begin{aligned} H^{\sigma\sigma'}_{\mu\nu\{\underline{\mathbf{g}}\}} &\equiv \langle \chi^{\sigma}_{\mu\{\underline{\mathbf{0}}\}} | \hat{\mathbf{H}} | \chi^{\sigma'}_{\nu\{\underline{\mathbf{g}}\}} \rangle \\ &= \int d\underline{\mathbf{r}}\ \chi_{\mu}(\underline{\mathbf{r}} - \underline{\mathbf{a}}_{\mu}) \boldsymbol{\sigma}^{T} \hat{\mathbf{H}} \boldsymbol{\sigma'} \chi_{\nu}(\underline{\mathbf{r}} - \underline{\mathbf{g}} - \underline{\mathbf{a}}_{\nu}) \end{aligned} \quad (6)$$

where σ, $\sigma' = \alpha$, β and $\boldsymbol{\sigma}$, $\boldsymbol{\sigma'} = \boldsymbol{\alpha}$, $\boldsymbol{\beta}$, $\hat{\mathbf{H}}$ is the Hamiltonian operator, which has a 2×2 structure in spin space and T is the transpose operator. The matrix elements above can be written as the following sum of terms:

$$H^{\sigma\sigma'}_{\mu\nu\{\underline{\mathbf{g}}\}} = h^{\sigma\sigma'}_{\mu\nu\{\underline{\mathbf{g}}\}} + b^{\sigma\sigma'}_{\mu\nu\{\underline{\mathbf{g}}\}} + C^{\sigma\sigma'}_{\mu\nu\{\underline{\mathbf{g}}\}} + aK^{\sigma\sigma'}_{\mu\nu\{\underline{\mathbf{g}}\}} + V^{\sigma\sigma'}_{\mu\nu\{\underline{\mathbf{g}}\}} , \quad (7)$$

where $\hat{\mathbf{h}}$ is the SR monoelectronic operator, $\hat{\mathbf{b}}$ is the SOC operator, $\hat{\mathbf{C}}$ is the Coulomb (or Hartree) operator, $\hat{\mathbf{K}}$ is the exact Fock exchange operator, a is the fraction of exact Fock exchange and $\hat{\mathbf{V}}$ is the exchange-correlation (xc) operator, written as a sum of exchange $\hat{\mathbf{V}}_x$ and correlation $\hat{\mathbf{V}}_c$ contributions:

$$\hat{\mathbf{V}} = (1-a)\hat{\mathbf{V}}_x + \hat{\mathbf{V}}_c . \quad (8)$$

Eqs. (7) and (8) reduce to the corresponding GHF expressions for $a = 1$ and $\hat{\mathbf{V}}_c = \mathbf{0}$. By exploitation of translational invariance, it can be shown that the Hamiltonian matrix is complex-Hermitian, such that the following relation holds for its matrix elements follows:

$$H^{\sigma\sigma'}_{\mu\nu\{\underline{\mathbf{g}}\}} = \left[H^{\sigma'\sigma}_{\nu\mu\{-\underline{\mathbf{g}}\}} \right]^{*} . \quad (9)$$

As a consequence, all other matrix elements in Eq. (7) also have the same property. For the Fock exchange operator, this is the only relation among its matrix elements. On the contrary, from the specific expressions of all other operators in the Hamiltonian, it is possible to derive further symmetry relations that can be exploited in the construction of the full matrix. For the Coulomb term, the matrix is real-Hermitian and block-diagonal in spin space, such that the following properties hold for its matrix elements:

$$C^{\sigma\sigma}_{\mu\nu\{\underline{\mathbf{g}}\}} = C^{\sigma\sigma}_{\nu\mu\{-\underline{\mathbf{g}}\}} = C^{\sigma'\sigma'}_{\mu\nu\{\underline{\mathbf{g}}\}} = C^{\sigma'\sigma'}_{\nu\mu\{-\underline{\mathbf{g}}\}} . \quad (10)$$

The matrix elements $h^{\sigma\sigma'}_{\mu\nu\{\underline{\mathbf{g}}\}}$ of the SR mono-electronic operator exhibit the same features of the Coulomb operator. For the xc operator, the matrix within each spin block is complex-symmetric:

$$V^{\sigma\sigma'}_{\mu\nu\{\underline{\mathbf{g}}\}} = V^{\sigma\sigma'}_{\nu\mu\{-\underline{\mathbf{g}}\}} = \left[V^{\sigma'\sigma}_{\mu\nu\{\underline{\mathbf{g}}\}} \right]^{*} = \left[V^{\sigma'\sigma}_{\nu\mu\{-\underline{\mathbf{g}}\}} \right]^{*} . \quad (11)$$

Finally, for the SOC operator, the diagonal spin-blocks are purely imaginary and each spin-block is anti-symmetric, such that the matrix elements satisfy the following relations:

$$b^{\alpha\alpha}_{\mu\nu\{\underline{\mathbf{g}}\}} = -b^{\alpha\alpha}_{\nu\mu\{-\underline{\mathbf{g}}\}} = -b^{\beta\beta}_{\mu\nu\{\underline{\mathbf{g}}\}} = b^{\beta\beta}_{\nu\mu\{-\underline{\mathbf{g}}\}} , \quad (12)$$

and for the off-diagonal ($\sigma \neq \sigma'$) spin-blocks, they are complex-anti-symmetric:

$$b^{\alpha\beta}_{\mu\nu\{\underline{\mathbf{g}}\}} = -b^{\alpha\beta}_{\nu\mu\{-\underline{\mathbf{g}}\}} = -\left[b^{\beta\alpha}_{\mu\nu\{\underline{\mathbf{g}}\}} \right]^{*} = \left[b^{\beta\alpha}_{\nu\mu\{-\underline{\mathbf{g}}\}} \right]^{*} . \quad (13)$$

In the present implementation, we make explicit use of all the relations among matrix elements from Eqs. (9)-(13), such that we compute and store in memory explicitly only a fraction of the total number of matrix elements (at most half of them, for the Fock exchange operator).

2. Matrix Elements in Momentum Space

Hamiltonian matrix elements in momentum space are written using the following compact notation:

$$\begin{aligned} H^{\sigma\sigma'}_{\mu\nu\{\underline{\mathbf{k}}\}} &\equiv \Omega_r \langle \phi^{\sigma}_{\mu\{\underline{\mathbf{k}}\}} | \hat{\mathbf{H}} | \phi^{\sigma'}_{\nu\{\underline{\mathbf{k}}\}} \rangle \\ &= \Omega_r \int d\underline{\mathbf{r}}\ \phi^{*}_{\mu}(\underline{\mathbf{r}}; \underline{\mathbf{k}}) \boldsymbol{\sigma}^{T} \hat{\mathbf{H}} \boldsymbol{\sigma'} \phi_{\nu}(\underline{\mathbf{r}}; \underline{\mathbf{k}}) . \end{aligned} \quad (14)$$

The matrix elements in momentum space are obtained as a Fourier transform of those in position space:

$$H^{\sigma\sigma'}_{\mu\nu\{\underline{\mathbf{k}}\}} = \sum_{\underline{\mathbf{g}}} H^{\sigma\sigma'}_{\mu\nu\{\underline{\mathbf{g}}\}} e^{i\underline{\mathbf{k}}\cdot\underline{\mathbf{g}}} , \quad (15)$$

where the sum runs over all lattice vectors. To facilitate the generalization of existing SR programs, instead of using directly Eq. (15), it is advantageous to first transform individually the real and imaginary parts of the position space matrix elements:

$${}^{R}H^{\sigma\sigma'}_{\mu\nu\{\underline{\mathbf{k}}\}} = \sum_{\underline{\mathbf{g}}} \Re \left[H^{\sigma\sigma'}_{\mu\nu\{\underline{\mathbf{g}}\}} \right] e^{i\underline{\mathbf{k}}\cdot\underline{\mathbf{g}}} , \quad (16)$$

and:

$$ {}^{I}H^{\sigma\sigma'}_{\mu\nu\{\underline{\mathbf{k}}\}} = \sum_{\underline{\mathbf{g}}} \Im\left[H^{\sigma\sigma'}_{\mu\nu\{\underline{\mathbf{g}}\}}\right] e^{i\underline{\mathbf{k}}\cdot\underline{\mathbf{g}}} \, . \tag{17} $$

We stress that both quantities on the lhs of Eqs. (16) and (17) are complex while the superscripts R and I only refer to the pure real and pure imaginary character of the objects being transformed on the corresponding rhs. These complex quantities can then be combined to form the real and imaginary parts of the matrix elements in momentum space as follows:

$$ \Re\left[H^{\sigma\sigma'}_{\mu\nu\{\underline{\mathbf{k}}\}}\right] = \Re\left[{}^{R}H^{\sigma\sigma'}_{\mu\nu\{\underline{\mathbf{k}}\}}\right] - \Im\left[{}^{I}H^{\sigma\sigma'}_{\mu\nu\{\underline{\mathbf{k}}\}}\right] \, , \tag{18} $$

and

$$ \Im\left[H^{\sigma\sigma'}_{\mu\nu\{\underline{\mathbf{k}}\}}\right] = \Im\left[{}^{R}H^{\sigma\sigma'}_{\mu\nu\{\underline{\mathbf{k}}\}}\right] + \Re\left[{}^{I}H^{\sigma\sigma'}_{\mu\nu\{\underline{\mathbf{k}}\}}\right] \, . \tag{19} $$

From the Hermiticity of the Hamiltonian matrix in position space (9), it follows that the Hamiltonian matrix is complex Hermitian for each point $\underline{\mathbf{k}}$ in momentum space:

$$ H^{\sigma\sigma'}_{\mu\nu\{\underline{\mathbf{k}}\}} = \left[H^{\sigma'\sigma}_{\nu\mu\{\underline{\mathbf{k}}\}}\right]^{*} \, . \tag{20} $$

3. The Density Matrix

Once the secular equations (5) have been solved in momentum space by diagonalization of the Hamiltonian matrix at a set of $\underline{\mathbf{k}}$ points on a Monkhorst-Pack mesh, complex two-component COs with coefficients $c^{\sigma}_{\mu i\{\underline{\mathbf{k}}\}}$ are obtained, and with corresponding energies $\epsilon_{i\{\underline{\mathbf{k}}\}}$. The occupied bands are then determined through the *aufbau* principle. For metallic systems, the Fermi energy ϵ_F must also be determined. This is achieved by numerical quadrature over the volume of the first Brillouin zone Ω_r of the Heaviside step functions $q(\underline{\mathbf{k}}) = \sum_i \theta[\epsilon_F - \epsilon_{i\{\underline{\mathbf{k}}\}}]$, with the index i running over all bands. The correct value of the Fermi energy ϵ_F is the value for which the numerical quadrature $\int_{\Omega_r} q(\underline{\mathbf{k}}) d\underline{\mathbf{k}}$ gives the number of electrons in the cell times Ω_r. More algorithmic details on how to efficiently perform the required numerical quadrature are presented in Ref. 63. In the existing 1c procedure for TRSB systems, the *aufbau* and numerical quadrature procedures are performed separately, first on the n pure α and then on the n pure β spin states. The extension to the treatment of 2c spinors involves instead performing the two procedures on the whole set of $2n$ mixed spin states. The density matrix $P^{\sigma\sigma'}_{\mu\nu\{\underline{\mathbf{k}}\}}$ is subsequently constructed from the occupied COs in momentum space, as follows:

$$ P^{\sigma\sigma'}_{\mu\nu\{\underline{\mathbf{k}}\}} = \frac{1}{\Omega_r} \sum_{i}^{occ} [c^{\sigma}_{\mu i\{\underline{\mathbf{k}}\}}]^{*} c^{\sigma'}_{\nu i\{\underline{\mathbf{k}}\}} \theta[\epsilon_F - \epsilon_{i\{\underline{\mathbf{k}}\}}] \, . \tag{21} $$

Finally, the density matrix must be back-Fourier transformed to position space:

$$ P^{\sigma\sigma'}_{\mu\nu\{\underline{\mathbf{g}}\}} = \int_{\Omega_r} d\underline{\mathbf{k}} \; P^{\sigma\sigma'}_{\mu\nu\{\underline{\mathbf{k}}\}} e^{i\underline{\mathbf{k}}\cdot\underline{\mathbf{g}}} \, , \tag{22} $$

because this latter quantity is used in the construction of the Hamiltonian matrix for the next self-consistent field (SCF) cycle. In Appendix A, we provide working expressions for constructing the real and imaginary parts of the position space density matrix from the occupied COs.

B. Time Reversal Symmetry Breaking in Momentum Space

1. General Considerations

The reversal of time has a well-established effect on position, electron momentum and spin, as follows:[9,64]

$$ \underline{\mathbf{r}} \mapsto \underline{\mathbf{r}} \tag{23a} $$
$$ \underline{\mathbf{k}} \mapsto -\underline{\mathbf{k}} \tag{23b} $$
$$ \alpha \mapsto \beta \tag{23c} $$
$$ \beta \mapsto -\alpha \, . \tag{23d} $$

Eq. (24) gives the following representation of the time-reversal operator in a two-component spinor basis:[9]

$$ \hat{\boldsymbol{\mathcal{T}}} = -i\hat{\boldsymbol{\sigma}}_y \hat{\mathcal{K}} = \begin{pmatrix} 0 & -1 \\ 1 & 0 \end{pmatrix} \hat{\mathcal{K}} \, , \tag{24} $$

where $\hat{\mathcal{K}}$ represents the complex-conjugation operator and the $\hat{\boldsymbol{\sigma}}_c$ are the complex 2×2 Pauli matrices, with $c = x, y, z$ being a Cartesian index. Substituting Eq. (24) in Eq. (14), we obtain the following for the action of $\hat{\boldsymbol{\mathcal{T}}}$ on the elements of the Hamiltonian matrix. For diagonal spin-blocks:

$$ \begin{aligned} \langle \phi^{\sigma}_{\mu\{\underline{\mathbf{k}}\}} | \hat{\boldsymbol{\mathcal{T}}}^{\dagger} \hat{\mathbf{H}} \hat{\boldsymbol{\mathcal{T}}} | \phi^{\sigma}_{\nu\{\underline{\mathbf{k}}\}} \rangle &\equiv \langle \hat{\boldsymbol{\mathcal{T}}} \phi^{\sigma}_{\mu\{\underline{\mathbf{k}}\}} | \hat{\mathbf{H}} | \hat{\boldsymbol{\mathcal{T}}} \phi^{\sigma}_{\nu\{\underline{\mathbf{k}}\}} \rangle \\ &= \langle \phi^{\sigma'}_{\mu\{-\underline{\mathbf{k}}\}} | \hat{\mathbf{H}} | \phi^{\sigma'}_{\nu\{-\underline{\mathbf{k}}\}} \rangle \, , \end{aligned} \tag{25} $$

and for off-diagonal spin-blocks:

$$ \begin{aligned} \langle \phi^{\sigma}_{\mu\{\underline{\mathbf{k}}\}} | \hat{\boldsymbol{\mathcal{T}}}^{\dagger} \hat{\mathbf{H}} \hat{\boldsymbol{\mathcal{T}}} | \phi^{\sigma'}_{\nu\{\underline{\mathbf{k}}\}} \rangle &\equiv \langle \hat{\boldsymbol{\mathcal{T}}} \phi^{\sigma}_{\mu\{\underline{\mathbf{k}}\}} | \hat{\mathbf{H}} | \hat{\boldsymbol{\mathcal{T}}} \phi^{\sigma'}_{\nu\{\underline{\mathbf{k}}\}} \rangle \\ &= -\langle \phi^{\sigma'}_{\mu\{-\underline{\mathbf{k}}\}} | \hat{\mathbf{H}} | \phi^{\sigma}_{\nu\{-\underline{\mathbf{k}}\}} \rangle \, , \end{aligned} \tag{26} $$

where in Eqs. (25) and (26), we assume that $\sigma \neq \sigma'$. Indeed, Eqs. (25) and (26) show that for open-shell systems time-reversal symmetry is broken because of the presence of unpaired electrons. As an example of this, let us suppose that the Hamiltonian commutes with the time-reversal operator (so that $\hat{\boldsymbol{\mathcal{T}}}^{\dagger} \hat{\mathbf{H}} \hat{\boldsymbol{\mathcal{T}}} = \hat{\mathbf{H}}$), then Eq. (25) would imply:

$$ H^{\alpha\alpha}_{\mu\nu\{\underline{\mathbf{k}}\}} = H^{\beta\beta}_{\mu\nu\{-\underline{\mathbf{k}}\}} \, . \tag{27} $$

Clearly Eq. (27) is not satisfied for open-shell systems, where the Hamiltonian matrix elements of α spinors cannot be related to those of β spinors.

Another aspect that is relevant to this discussion is space inversion symmetry. In inversion symmetric systems, the band structure at $\underline{\mathbf{k}}$ equals that at $-\underline{\mathbf{k}}$. The computational consequence of the latter is that, for systems with space inversion symmetry, the secular equations need not be explicitly built and diagonalised at both $\underline{\mathbf{k}}$ and $-\underline{\mathbf{k}}$. However, if the system does not exhibit space inversion symmetry, and if time-reversal symmetry is broken, there are in general no relations between the energy levels or matrix elements at $\underline{\mathbf{k}}$ and $-\underline{\mathbf{k}}$. So in absence of time-reversal and space inversion symmetries, the computational consequence is that the secular equations need to be explicitly built and diagonalised at both $\underline{\mathbf{k}}$ and $-\underline{\mathbf{k}}$.

A special exception to the above discussion is represented by the SR case (i.e. in the absence of SOC), where the Hamiltonian matrix elements $\tilde{H}^{\sigma}_{\mu\nu\{\underline{\mathbf{g}}\}}$ are purely real in position space so that one may write:

$$\begin{aligned}\tilde{H}^{\sigma}_{\mu\nu\{-\underline{\mathbf{k}}\}} &= \sum_{\underline{\mathbf{g}}} \tilde{H}^{\sigma}_{\mu\nu\{\underline{\mathbf{g}}\}} e^{-i\underline{\mathbf{k}}\cdot\underline{\mathbf{g}}} \\ &= \left[\sum_{\underline{\mathbf{g}}} \tilde{H}^{\sigma}_{\mu\nu\{\underline{\mathbf{g}}\}} e^{i\underline{\mathbf{k}}\cdot\underline{\mathbf{g}}}\right]^{*} = \left[\tilde{H}^{\sigma}_{\mu\nu\{\underline{\mathbf{k}}\}}\right]^{*} . \quad (28)\end{aligned}$$

So the matrix-elements at opposite points in momentum space form complex-conjugate pairs. It is straightforward to show that this implies that the energy levels at opposite points in momentum space are equivalent (i.e. $\epsilon^{\sigma}_{i\{\underline{\mathbf{k}}\}} = \epsilon^{\sigma}_{i\{-\underline{\mathbf{k}}\}}$) and the COs are complex-conjugate pairs (i.e. $c^{\sigma}_{\mu i\{\underline{\mathbf{k}}\}} = [c^{\sigma}_{\mu i\{-\underline{\mathbf{k}}\}}]^{*}$). Hence, the secular equations need not be diagonalised at opposite points in momentum space in the special case where the Hamiltonian is purely real in position space (i.e. for SR calculations). However, this is not true in the presence of SOC, where the Hamiltonian matrix is necessarily complex in position space, and therefore the secular equations need to be explicitly built and diagonalised at both $\underline{\mathbf{k}}$ and $-\underline{\mathbf{k}}$, if the system lacks time-reversal and space inversion symmetry.

2. The Effect of Fock Exchange

The need to explicitly diagonalize the secular equations at both $\underline{\mathbf{k}}$ and $-\underline{\mathbf{k}}$ is generally true for any Hamiltonian including SOC, provided that the system breaks both time-reversal and space inversion symmetries. Therefore, the electronic band structure of open-shell non-centrosymmetric periodic systems will exhibit different features at opposite $\underline{\mathbf{k}}$ points in the presence of SOC.

However, we show below that those KS-DFT Hamiltonians which do not include a fraction of exact non-local Fock exchange (i.e. plain formulations of the xc functionals) are constrained in the manner in which they allow time-reversal symmetry breaking. Instead, the presence of a fraction of exact non-local Fock exchange in the functional (such as in hybrid xc functionals) removes such constraints and allows for a full breaking of the time-reversal symmetry in momentum space. From the symmetry properties of the matrix elements discussed in Section II A 1, we show (the demonstration is reported in the ESI)[65] that KS-DFT Hamiltonians based on plain (non hybrid) xc functionals provide band structures which are constrained by the following sum-rule:

$$\sum_i \epsilon_{i\{\underline{\mathbf{k}}\}} = \sum_i \epsilon_{i\{-\underline{\mathbf{k}}\}} , \quad (29)$$

where the sums run over all electronic energy levels. On the other hand, for GKS-DFT Hamiltonians including a fraction of Fock exchange, the above constraint on the breaking of time-reversal symmetry is lost:

$$\sum_i \epsilon_{i\{\underline{\mathbf{k}}\}} \neq \sum_i \epsilon_{i\{-\underline{\mathbf{k}}\}} . \quad (30)$$

C. Time Reversal Symmetry Breaking in Position Space

A well-defined fully relativistic formulation exists for treating TRSB systems from the DFT, based on appropriate density variables.[12,13,31,32,46,47] In particular, from the SCDFT, it has been shown that in the 2c approach the appropriate density variables from which functionals have to be built are first the particle-number density n:

$$n(\underline{\mathbf{r}}) = \sum_i^{occ} \int_{\Omega'_r} d\underline{\mathbf{k}}\ \underline{\mathbf{\Psi}}^{\dagger}_i(\underline{\mathbf{r}};\underline{\mathbf{k}})\underline{\mathbf{\Psi}}_i(\underline{\mathbf{r}};\underline{\mathbf{k}}) , \quad (31)$$

where Ω'_r represents the subset of points in momentum space inside Ω_r for which $\epsilon_{i\{\underline{\mathbf{k}}\}} \leq \epsilon_F$. The second density variable from which 2c functionals are to be built for TRSB systems is the magnetization $\underline{\mathbf{m}}$. Its Cartesian components are denoted as m_c, with $c = x, y, z$ being a Cartesian index. They are defined as follows in terms of 2c spinor COs:

$$m_c(\underline{\mathbf{r}}) = \sum_i^{occ} \int_{\Omega'_r} d\underline{\mathbf{k}}\ \underline{\mathbf{\Psi}}^{\dagger}_i(\underline{\mathbf{r}};\underline{\mathbf{k}})\hat{\boldsymbol{\sigma}}_c\underline{\mathbf{\Psi}}_i(\underline{\mathbf{r}};\underline{\mathbf{k}}) . \quad (32)$$

The third variable is the orbital-current density $\underline{\mathbf{j}}$:[13,14]

$$\begin{aligned}\underline{\mathbf{j}}(\underline{\mathbf{r}}) = \frac{1}{2i}\sum_i^{occ} \int_{\Omega'_r} d\underline{\mathbf{k}}\ \underline{\mathbf{\Psi}}^{\dagger}_i(\underline{\mathbf{r}};\underline{\mathbf{k}}) \left[\underline{\boldsymbol{\nabla}}\underline{\mathbf{\Psi}}_i(\underline{\mathbf{r}};\underline{\mathbf{k}})\right] \\ - \left[\underline{\boldsymbol{\nabla}}\underline{\mathbf{\Psi}}_i(\underline{\mathbf{r}};\underline{\mathbf{k}})\right]^{\dagger} \underline{\mathbf{\Psi}}_i(\underline{\mathbf{r}};\underline{\mathbf{k}}) , \quad (33)\end{aligned}$$

where the $\underline{\boldsymbol{\nabla}}$ indicates the gradient over the position variable $\underline{\mathbf{r}}$.

Finally, the functional must also depend on the three spin-current density vectors $\underline{\mathbf{J}}_x$, $\underline{\mathbf{J}}_y$, and $\underline{\mathbf{J}}_z$:[31,32]

$$\begin{aligned}\underline{\mathbf{J}}_c(\underline{\mathbf{r}}) = \frac{1}{2i}\sum_i^{occ} \int_{\Omega'_r} d\underline{\mathbf{k}}\ \underline{\mathbf{\Psi}}^{\dagger}_i(\underline{\mathbf{r}};\underline{\mathbf{k}})\hat{\boldsymbol{\sigma}}_c \left[\underline{\boldsymbol{\nabla}}\underline{\mathbf{\Psi}}_i(\underline{\mathbf{r}};\underline{\mathbf{k}})\right] \\ - \left[\underline{\boldsymbol{\nabla}}\underline{\mathbf{\Psi}}_i(\underline{\mathbf{r}};\underline{\mathbf{k}})\right]^{\dagger} \hat{\boldsymbol{\sigma}}_c\underline{\mathbf{\Psi}}_i(\underline{\mathbf{r}};\underline{\mathbf{k}}) , \quad (34)\end{aligned}$$

To perform GKS-DFT calculations, we have to deal with the problem that unfortunately there is a lack of any explicit relativistic functional within the 2c approach for TRSB systems, as recalled in the introduction.[12–17] We stress that also within the most general 4c approach, where the appropriate density variable is the so-called four-current $\boldsymbol{\mathcal{J}}$, no explicit functionals have been devised for TRSB systems.[12,13,47]

Therefore, in practice, DFT relativistic calculations on TRSB systems must be performed by modifying existing non-relativistic 1c functionals using appropriate collinear formulations (in which the functional depends only on n and m_z) or non-collinear formulations (in which the functional depends only on n and $\underline{\mathbf{m}}$).[9,16,18–30] So, even though non-collinear formulations introduce the dependence of the functionals on n and $\underline{\mathbf{m}}$, a problem remains for the inclusion of $\underline{\mathbf{j}}$ and the $\underline{\mathbf{J}}_c$ in the two-electron potential. One work-around to this problem would be generalizing scalar-relativistic functionals designed for calculations in the presence of external fields to perform 2c calculations.[33–40] Although technically possible, the question remains open as to whether such a procedure would result in a successful relativistic calculation. Furthermore, while these introduce the dependence on the orbital-current density $\underline{\mathbf{j}}$, they do not include the $\underline{\mathbf{J}}_c$. Another approach would be to replace the dependence on the kinetic-energy density τ of meta-GGA functionals with a function of the orbital-current density $\tau \rightarrow f\left(\underline{\mathbf{j}} \cdot \underline{\mathbf{j}}\right)$.[41] Here, however, we do not follow this possible direction because of the diverse challenges it would pose, related to the simultaneous treatment of both $\underline{\mathbf{j}}$ and $\underline{\mathbf{m}}$, as already elaborated in the introduction. We therefore discuss the treatment of $\underline{\mathbf{j}}$ and the $\underline{\mathbf{J}}_c$ solely from the exact non-local Fock exchange operator.

We have recently shown that the particle-number density n and magnetization $\underline{\mathbf{m}}$ are built from, and therefore depend on, most spin-blocks of the complex density matrix, but not the $\alpha\alpha$ and $\beta\beta$ diagonal imaginary ones. At the same time, these two blocks are those which enter the definition of the orbital-current density $\underline{\mathbf{j}}$.[17] A detailed demonstration on how the $\underline{\mathbf{j}}$ can be shown to depend on the sum of the $\alpha\alpha$ and $\beta\beta$ (denoted as $\alpha\alpha \oplus \beta\beta$) diagonal imaginary spin blocks of the density matrix is reported in Appendix B. We stress that these blocks arise from the presence of a SOC operator in the Hamiltonian. From Appendix B it is shown that the n, $\underline{\mathbf{m}}$ and $\underline{\mathbf{j}}$ introduce the dependence on all spin-blocks of the density matrix, except for a remaining three blocks (namely, the imaginary part of the sum of the off-diagonal spin-blocks $\beta\alpha \oplus \alpha\beta$ and the difference of the diagonal spin blocks $\alpha\alpha \ominus \beta\beta$, as well as the real part of the $\beta\alpha \ominus \alpha\beta$ block). This brings us to Appendix C, where it is shown that these remaining three spin-blocks of the density matrix define the spin-current density vectors $\underline{\mathbf{J}}_x$, $\underline{\mathbf{J}}_y$ and $\underline{\mathbf{J}}_z$. It follows that while a hypothetical xc functional built from n, $\underline{\mathbf{m}}$, $\underline{\mathbf{j}}$ and the $\underline{\mathbf{J}}_c$ would ensure the correct dependence of the two-electron potential on all blocks of the density matrix (i.e. on all pieces of the wave-function), an xc functional built solely from n and $\underline{\mathbf{m}}$ does not.

1. *The Role of Fock Exchange*

As a matter of fact, in practical relativistic DFT, the Fock exchange is the only two-electron operator which introduces a dependence on the otherwise missing four spin-blocks of the density matrix (imaginary part of the $\alpha\alpha \oplus \beta\beta$, $\alpha\alpha \ominus \beta\beta$ and $\beta\alpha \oplus \alpha\beta$ blocks, as well as real part of the $\beta\alpha \ominus \alpha\beta$ block) discussed above into the two-electron potential. The practical consequence of all this, as we have recently shown for the case of the orbital-current density $\underline{\mathbf{j}}$,[17] is that for relativistic calculations including SOC, a non-vanishing fraction of Fock exchange (as done with hybrid xc functionals) is necessary to allow proper coupling of the magnetization with the orbital- and spin-current densities. In Section IV, we provide numerical examples to complement this formal analysis, where we show that both the orbital-current density and magnetization have unphysical distributions from non-hybrid functional calculations. In these examples, the inclusion of a sufficiently large fraction of exact non-local Fock exchange remedies this problem.

Finally, we also discuss another formal advantage of using hybrid functionals, that is the ability of the exact Fock exchange operator to provide a local magnetic torque (LMT).[30,48,66] The LMT represents the ability of the two-electron potential to locally rotate the magnetization during the SCF procedure, with respect to a starting guess configuration. For plain (i.e. non-hybrid) formulations of the DFT, the part of two-electron potential which yields a non-vanishing contribution to the LMT corresponds to the so-called xc magnetic field $\underline{\boldsymbol{\mathcal{B}}}_{\mathrm{xc}}$, and in this case the LMT is sometimes called the xc torque.[49,50,67] In principle, non-collinear formulations of the DFT could also be devised in such a way to locally provide a non-vanishing LMT. In fact, this is the case for the non-collinear formulation of Scalmani and Frisch.[24] We have, however recently shown that such formulations as they currently exist are not rotationally invariant.[16] As a result, exact Fock exchange is necessary to provide a non-vanishing LMT within the context of a rotationally invariant theory.

III. COMPUTATIONAL DETAILS

The calculations are performed on a model 1D periodic system with both space inversion and time-reversal symmetries broken. The model is a modified poly-acetylene (C_2H_2) polymer, whose structure was obtained as follows. We replaced the two C atoms in the primitive unit cell with Ge atoms to enhance SOC and we removed one H atom from the cell, as this allows us to obtain an open-shell electronic ground state configuration. The final stoichiometry of the model system thus reads Ge_2H,

with three atoms in the primitive unit cell and a lattice parameter of 2.464 Å.

All calculations are performed with our self-consistent treatment of SOC in a two-component spinor basis,[16,48] as implemented in a developmental version of the CRYSTAL17 code.[59,68] Crystalline orbitals are expressed as a linear combination of atom-centered atomic orbitals.[60] For H, we use the all-electron basis set by Dovesi and co-workers,[69] while for Ge, we use the fully relativistic (scalar + spin-orbit) effective-core pseudo-potential ECP28MDF by Dolg and co-workers along with the corresponding (5s4p)/[3s2p] valence basis-set.[70] Convergence is achieved when the difference in energy between two successive cycles does not exceed 1×10^{-12} a.u. Calculations are performed using the SVWN5 exchange-correlation (xc) functional of the LDA and the PBE xc functional of the GGA.[71–73] For GGA calculations, we use our signed-canonical formulation of non-collinear DFT, which, at variance with other existing formulations, guarantees rotational invariance of the total energy.[16] For GGA calculations, we also accelerate the SCF with the dynamical damping method (also known as optimal damping algorithm or relaxed constraints algorithm) proposed by Karlström and Cancès,[74–76] which we have generalized to a 2c SCF.

The numerical integration required for calculating the xc energy and matrix elements is performed using an unpruned grid containing 75 radial points and a Lebedev accuracy level of 16, corresponding to 974 angular points for each radial point, and the quadrature weights proposed by Becke.[77–80] Integration of the density matrix and diagonalization of the Fock matrix is performed in reciprocal space, with sampling on 30 points. A Fermi smearing was applied with a smearing width of 1×10^{-3} a.u. Truncation of the Coulomb and exchange infinite lattice series is controlled by five parameters, which are here set to 8 8 8 8 20 (keyword `TOLINTEG`, see user's manual for more details).[81] The initial guess magnetization is obtained from a SR atomic Hartee-Fock calculation and rotated, using an approach which we discuss elsewhere.[48] The orientation of the vector $\underline{\mathbf{w}}$ in Eq. (60) of Ref. 48 (which roughly corresponds to the orientation of the guess magnetization on each atom) is along the xyz diagonal, unless otherwise specified.

IV. RESULTS AND DISCUSSION

In this section, we discuss the results of our fully relativistic DFT calculations on the Ge_2H chain, which serves as a simple model system where both space inversion and time-reversal symmetries are broken in a periodic lattice, in the presence of a SOC operator. We illustrate the practical consequences of the theoretical arguments already elaborated in Section II, and, in particular, the effect of including a fraction of non-local exact Fock exchange in the Hamiltonian. Specifically, we discuss:

- The LMT (i.e. ability to locally rotate the magnetization) imparted to the two-electron potential by the Fock exchange operator. The inability of the two-electron potential to rotate the magnetization during the self-consistent treatment of SOC in the absence of Fock exchange results in different guesses for the orientation of the initial magnetization yielding different final solutions. On the other hand, with hybrid xc functionals we are always able to find a consistent solution in terms of energy and spatial distribution of the magnetization, regardless of the starting guess.

- The improved rotational invariance of the total energy due to the LMT of the Fock operator in non-collinear GGA calculations.

- The effect of Fock exchange on the spatial distribution of the magnetization, orbital- and spin-current densities. Only the presence of the Fock exchange operator allows for the orbital- and spin-current densities to properly evolve along the SCF and to couple with the magnetization to yield physically meaningful solutions.

- The full breaking of the time-reversal symmetry in momentum space enabled by the presence of Fock exchange. Without it, a sum-rule constrains the electronic band structure at opposite points in reciprocal space thus preventing to reach some TRSB states.

A. The Local Magnetic Torque

The presence (or lack) of a LMT of the type discussed in Section II C 1 determines the ability (or inability) of the magnetization to evolve during the self-consistent treatment of SOC, and in particular to rotate in space (i.e. to change its orientation). As a matter of fact, a practical way to discuss the effect of the LMT is that of performing the same calculation by starting from different initial guesses for the orientation of the magnetization, and to analyze the corresponding final solutions. In this respect, we have recently developed a new approach for generalizing a non- or scalar-relativistic atomic guess density matrix to impose a desired non-collinear magnetization as a starting point of the SCF procedure.[48] This approach allows to define an initial atomic magnetization with a different orientation around each atom, and proves crucial to sample rugged energy landscapes.

We have performed three calculations by starting from three different orientations for the magnetization on each atomic center: a guess along x, one along yz, and one along xyz. Figure 1 shows the spatial distribution of the magnetization in the xy plane of the infinite Ge_2H chain as obtained at the end of the SCF procedure. Results on the left are from plain LDA while those on the right are from hybrid LDA (with 50% of Fock exchange). Later, in Section IV B, we will discuss the effect of different

fractions of Fock exchange on the magnetization, orbital- and spin-current density distributions. The small black arrows in the figure have length and orientation which reflect the magnitude and direction of the m_x and m_y components of the magnetization, while the color represents the modulus m of the magnetization vector. The energy difference of each solution with respect to that obtained with the initial guess along x is reported alongside each panel.

The figure shows that for the pure LDA calculations three different final solutions for the magnetization are obtained with the three different initial guesses. In fact, for each case, the final solution follows the orientation of the guess magnetization. On the contrary, with the hybrid LDA calculations, we are able to obtain the same final solution for the magnetization with the three different guesses. This is because, with the presence of a fraction of Fock exchange and the corresponding LMT, the two-electron potential is able to locally rotate the magnetization during the SCF procedure, such that the final solution is mostly independent of the starting guess. On the other hand, for the pure LDA calculation, the lack of LMT implies that the magnetization is not able to rotate during the SCF procedure in order to find the lowest energy solution. Indeed, it can be seen that the energy differences among the obtained solutions for the pure LDA calculations are consistently larger than those for the hybrid LDA calculations.

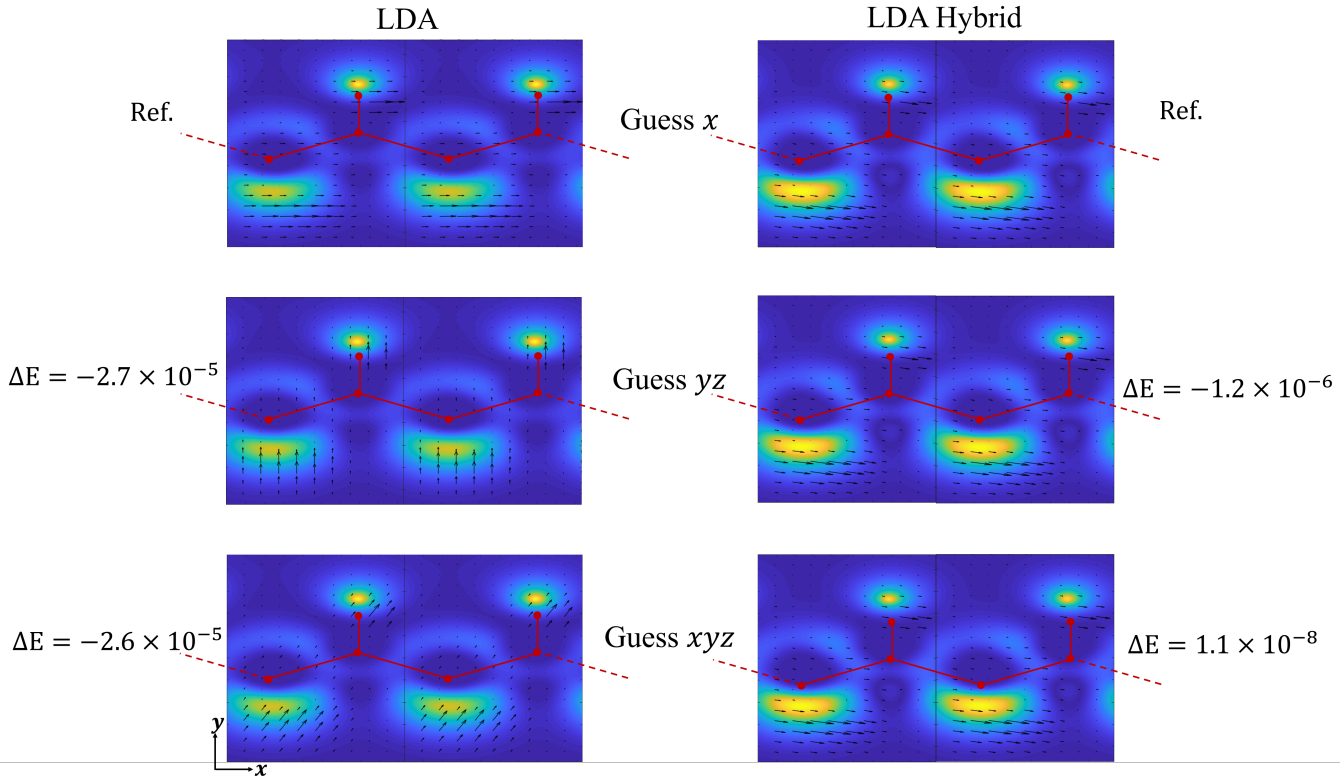

FIG. 1: Spatial distribution of the magnetization for LDA (left) and hybrid LDA (right) relativistic calculations on the Ge_2H infinite chain in the presence of SOC, as a function of the initial guess for the magnetization. The orientation of the guess magnetization on each atomic center is written in the center of the figure. The small black arrows in the figure have length and orientation which reflect the magnitude and direction of the m_x and m_y components of the magnetization, while the color represents the modulus m of the magnetization vector from blue (for small magnetization) to yellow (for large magnetization). The red ball-and-stick drawing represents the positions of the atoms. Energy differences w.r.t. the top panel are reported in eV.

1. *The Rotational Invariance for GGA Calculations*

The presence of a LMT imparted to the two-electron potential by Fock exchange also improves the rotational invariance of the total energy in non-collinear GGA calculations. The rotational invariance (i.e. the ability to get to the same solution for different orientations of the

system in space) is not ensured by the collinear formulation of the DFT. A non-collinear formulation is needed to restore it. However, this was only true for LDA functionals while all previously reported non-collinear formulations for GGA functionals suffered from the lack of rotational invariance. We have recently presented an alternative formulation for non-collinear GGA calculations, called "signed-canonical", which provides a rotationally-invariant potential.[16]

As an example of this, we performed two calculations with the PBE (including no fraction of Fock exchange) and PBE0 (including a 25% fraction of Fock exchange)[82] xc functionals of the GGA. Two equivalent geometries have been considered, which are linked by a rotation by 90 degrees along the periodic axis: in the first one the atoms of the Ge_2H infinite chain lie on the xy plane, while in the second on the xz plane. To ensure consistency, also the orientation of the guess magnetization has been rotated accordingly. In a perfectly rotationally-invariant theory, both calculations should yield the same energy, down to the convergence criterium of the SCF procedure. For these calculations, we set the convergence criterium to 10^{-7} a.u. For the PBE calculations, the energy difference between the two calculations is 1.3×10^{-5} a.u., which is two orders of magnitude higher than the convergence criterium. On the other hand, for the hybrid PBE0 calculations, the difference in energy between the two calculations is 5.0×10^{-10} a.u., so that the rotational invariance has improved by five orders of magnitude (down to the precision of the calculation) by including a fraction of Fock exchange.

B. Fock Exchange and the Current Densities

As discussed in Section II C, non-collinear xc functionals for relativistic DFT calculations should depend on the particle number density n, the magnetization $\underline{\mathbf{m}}$, the orbital-current density $\underline{\mathbf{j}}$ and the spin-current densities $\underline{\mathbf{J}}_c$. As a matter of fact, no existing functionals which can be applied to 2c calculations depend on $\underline{\mathbf{j}}$ and the $\underline{\mathbf{J}}_c$. We stress again that the previous statement excludes those $\underline{\mathbf{j}}$-dependent functionals for 1c finite external field calculations, whose successful generalization to the 2c case is yet to be shown.[33–41] The lack of such functionals leads to a two-electron potential that is independent of specific pieces of the wavefunction (in particular those mapped onto the imaginary part of the $\alpha\alpha \oplus \beta\beta$, $\alpha\alpha \ominus \beta\beta$ and $\beta\alpha \oplus \alpha\beta$ blocks, as well as the real part of the $\beta\alpha \ominus \alpha\beta$ block of the complex density matrix).[17] This has the practical consequence of allowing for a poor relaxation of the orbital- and spin-current densities along the SCF process, through a weak coupling with the magnetization. Fock exchange has the ability to introduce this missing dependence into the potential and therefore ensures a better description of the orbital- and spin-current densities, and, through a stronger coupling with $\underline{\mathbf{m}}$, of the magnetization itself.

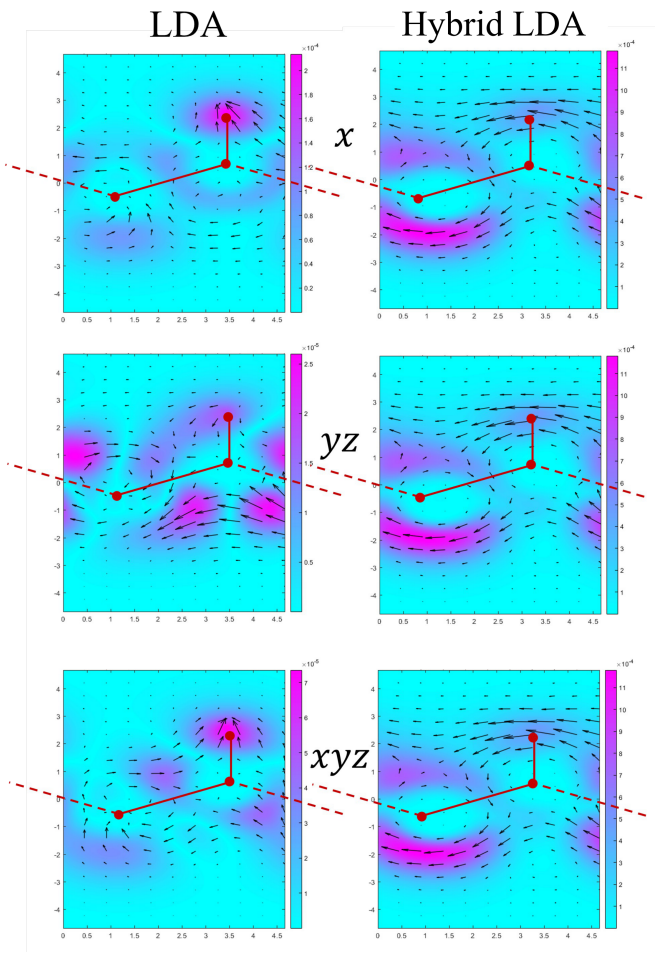

FIG. 2: Spatial distribution in the xy plane of the orbital-current density for LDA (left) and hybrid LDA (right) relativistic calculations on the Ge_2H infinite chain in the presence of SOC, as a function of the initial guess for the magnetization. The orientation of the guess magnetization on each atomic center is written in the center of the figure. The small black arrows in the figure have length and orientation which reflect the magnitude and direction of the j_x and j_y components of the orbital-current density, while the color represents the modulus j of the orbital-current density vector from light-blue (small values) to fucsia (large values). The red ball-and-stick drawing represents the positions of the atoms.

We have shown in Section IV A how heavily the final SCF solution depends on the initial guess for the magnetization in the absence of Fock exchange. This is even more so when it comes to the current densities for the formal reasons addressed in Section II C and briefly recalled above. We perform three relativistic calculations, with SOC, by starting the SCF procedure from three different initial guesses, as done in Section IV A. Figure 2 shows the spatial distribution of the orbital-current density in the xy plane of the infinite Ge_2H chain as obtained at the end of the SCF procedure. Results on the left are from plain LDA while those on the right are from hybrid LDA (with 50% of Fock exchange). The graphical representa-

tion follows the same conventions as for the magnetization in Figure 1. Inspection of Figure 2 shows how, for plain DFT calculations, the lack of the dependence of the two-electron potential on those specific pieces of the two-component spinor wavefunction discussed above results in the inability to relax the orbital-current density during the self-consistent evolution of the electronic ground state. Indeed, three different starting points result in three distinct final distributions for the orbital-current density. On the contrary, when a fraction of Fock exchange is included in the potential, we consistently find the same final solution regardless of the starting point because of the ability of the potential to relax the orbital- and spin-current densities. We believe that this analysis nicely shows how, in the context of practical relativistic DFT, the use of hybrid functionals in a fully self-consistent 2c framework is mandatory to get physically meaningful solutions, independent of the initial guess.

So far, we have discussed how Fock exchange allows for: i) the proper evolution of the magnetization along the SCF process because of the LMT it imparts; ii) the proper evolution of the orbital- and spin-current densities along the SCF process because of the dependence it imparts to the potential on the corresponding pieces of the wavefunction. These two aspects are not independent. Their simultaneous effect allows for the magnetization and orbital- and spin-current densities to couple and evolve jointly and in a physically consistent way along the SCF. We are going to show below how the final distributions of both magnetization and orbital-current density are affected by the fraction of Fock exchange included in the xc functional. In Figure 3, we report maps similar to those of Figures 1 and 2 for both the magnetization (top) and orbital-current density (bottom) obtained with different fractions of Fock exchange. Both quantities depend strongly on the fraction of Fock exchange.

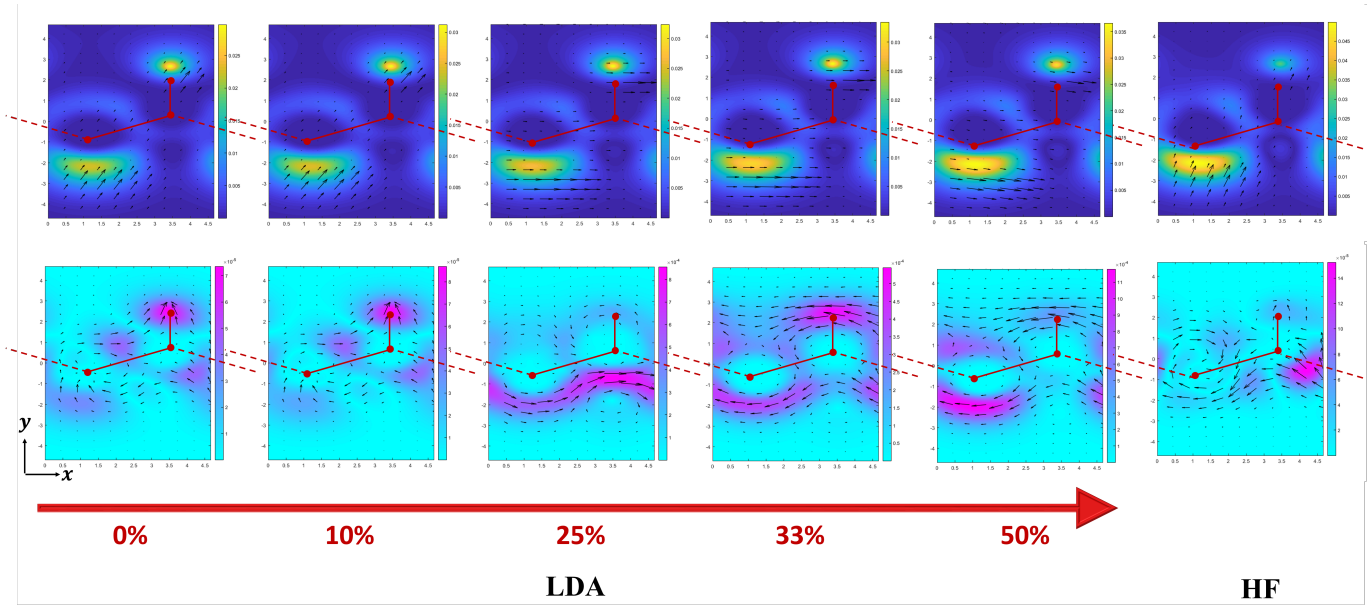

FIG. 3: Spatial distribution, in the xy plane, of the magnetization (top) and orbital-current density (bottom) for LDA and hybrid LDA calculations, with different fractions of Fock exchange, as well as for a Hartree-Fock (HF) calculation. The plotted quantities follow the same conventions described for Figure 1. The figure shows that both the magnetization and orbital-current density distributions depend strongly on the fraction of Fock exchange.

Let us analyze the distribution of the magnetization first. The color map clearly shows that, as expected, the region of maximum magnetization is that right below the first Ge atom (i.e. the one where the H atom was removed and an unpaired electron left). Some magnetization is built also close to the H atom.These features are common to all fractions of Fock exchange. The situation is different when it comes to the orientation of the magnetization. With a low fraction (for $a = 0\%$ and $a = 10\%$) the magnetization has a positive y component, whereas for high fractions of Fock exchange ($a = 50\%$) the magnetization has a negative y component. For intermediate fractions ($a = 25\%$ and $a = 33\%$) the magnetization has a small y component, so that the vectors point along the

TABLE I: Values (in eV) of the quantity Q, defined in Eq. (35), as a function of the fraction of Fock exchange, and as obtained with the SVWN5 functional of the LDA and the PBE functional of the GGA.

a [%]	0	10	25	33	50
LDA	10^{-10}	10^{-8}	10^{-1}	10^{-1}	10^{-1}
GGA	10^{-11}	10^{-4}	10^{-1}	10^{-1}	10^{-1}

periodic x direction.

With regards to the orbital-current density, Fock exchange is found to strongly affect both its orientation and spatial distribution. For small fractions of Fock exchange (for $a = 0\%$ and $a = 10\%$) it displays a large y component around the H atom. For large fractions of Fock exchange ($a = 33\%$ and $a = 50\%$) the orbital-current density instead points in the negative x direction around the H atom and also develops a large (in absolute value) negative x component below the Ge-Ge bond. For intermediate fractions ($a = 25\%$) the orbital-current density is instead small around the H atom and points in the positive x direction below the Ge-Ge bond.

For the periodic Hartree-Fock (HF) calculation, the magnetization has a positive y component, and the orbital-current density is largest under the Ge-Ge bond, where it points in the negative x direction. Unfortunately, we cannot say which fraction of Fock exchange most accurately reproduces the true distributions, because such an assertion would require an accurate, periodic, fully relativistic correlated wavefunction calculation, for which no implementation is yet available. We therefore leave such comparisons for future work. However, we have recently shown on a molecular system, for which comparison with accurate correlated methods is possible, how hybrid DFT calculations compare favorably with results from a reference spin-orbit configuration-interaction calculation, when an intermediate ($a = 20\%$ and $a = 25\%$) fraction of Fock exchange is used.[17] This also closely coincides with values of a typically used in non- or scalar-relativistic calculations.[82]

C. Full Breaking of Time-Reversal Symmetry in Momentum Space

In Section II B, we have shown how the presence of the Fock exchange operator in the Hamiltonian allows for the full breaking of time-reversal symmetry in momentum space. In its absence, the electronic band structure at opposite $\underline{\mathbf{k}}$ points would be constrained by the sum-rule in Eq. (29). To support the formal proof of the sum-rule discussed in Section II B 2 and in the ESI, here we perform numerical tests. Let us define the following quantity:

$$Q = \frac{1}{N_{\text{pairs}}} \sum_{\underline{\mathbf{k}}>0} \left| \sum_i \epsilon_{i\{\underline{\mathbf{k}}\}} - \epsilon_{i\{-\underline{\mathbf{k}}\}} \right| , \qquad (35)$$

where N_{pairs} is the number of pairs of opposite points ($\underline{\mathbf{k}}$ and $-\underline{\mathbf{k}}$) of sampling points in the first Brillouin zone, and the sum runs over the points with positive coordinates. From the sum-rule of Eq. (29), we expect that Q should be vanishingly small for non-hybrid xc functionals. Instead, for hybrid functionals, Q measures the degree to which the sum-rule is broken. Table I does indeed show that Q is vanishingly small in the absence of Fock exchange in the Hamiltonian, as the values reported are on the order of 10^{-10} eV for the LDA calculation and 10^{-11} eV for the PBE calculation. For small values of a, Q steadily increases for both the LDA and GGA calculations. Once a sufficiently high fraction a of Fock exchange is included in the functional (in this case higher than 10%), Q stabilizes to a value on the order of 10^{-1} eV, regardless of whether the LDA or GGA is used.

The consequence of the sum-rule is that a fraction of Fock exchange in the Hamiltonian is required to fully break time-reversal symmetry and access the full range of possible TRSB states. We highlight the consequences of all this by showing in Figure 4 the electronic band structure of the Ge_2H infinite chain in the vicinity of the Fermi level as obtained from hybrid and non-hybrid LDA calculations. For the hybrid calculation, we choose a fraction $a = 50\%$, as this results in a Hamiltonian which very closely resembles that of the previously reported Becke Half and Half (BHandH) functional.[83] Also, the choice of such a large value for a allows us to better highlight its effect. As expected, the SR calculations (i.e. in the absence of SOC) produce band structures which are symmetric about the Γ-point (dotted lines). For the hybrid calculation with SOC on the other hand, the valence band shows a considerable asymmetric splitting of the energy levels at opposite points in momentum space ($\underline{\mathbf{k}}$ vs. $-\underline{\mathbf{k}}$). The valence band is indeed the only band which shows appreciable splitting at opposite points in momentum space, indicating that this splitting can only be reproduced by breaking of the sum-rule. On the contrary, for the non-hybrid calculation with SOC, the valence band does not show similar splitting, and virtually overlaps with the one from the SR calculation in this case, because the sum-rule is satisfied.

V. CONCLUSIONS

We have discussed formal and computational aspects of two-component relativistic DFT calculations with the simultaneous self-consistent treatment of spin-orbit coupling (SOC) and non-local Fock exchange in periodic sys-

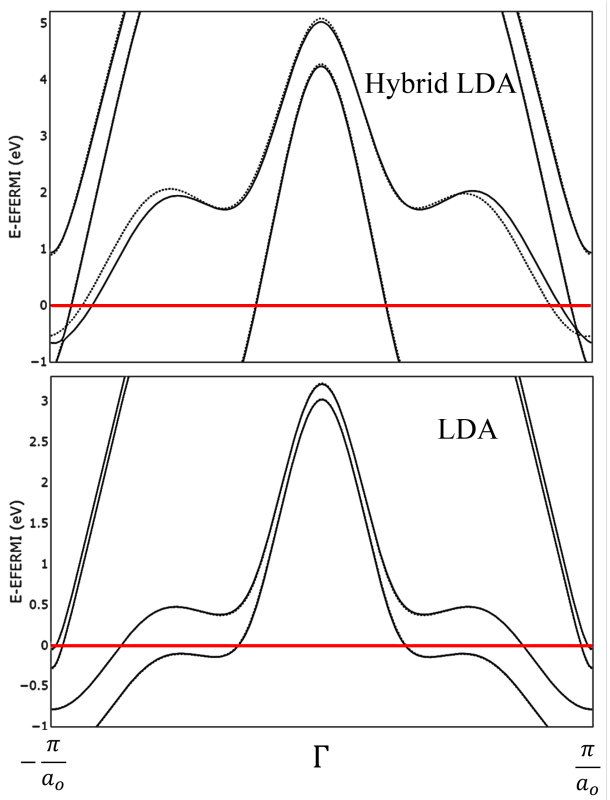

FIG. 4: Electronic band structure of the Ge_2H infinite chain from hybrid LDA (top) and non-hybrid LDA (bottom) calculations. The fraction of Fock exchange for the hybrid calculation is $a = 50\%$. The band structure from the fully relativistic calculation with the self-consistent treatment of SOC is plotted with solid lines, while that from a scalar-relativistic calculation (i.e. in the absence of SOC) is represented with dotted lines. The Fermi energy is set to zero and marked by a red horizontal line.

tems. In particular, we have presented the first implementation, in the public CRYSTAL code, of such methodology. The numerous fundamental advantages of including the non-local Fock exchange operator into the Hamiltonian for relativistic DFT calculations, as practically done in hybrid exchange-correlation functionals, have been introduced, which are particularly relevant to the study of time-reversal symmetry broken electronic configurations.

The Fock exchange operator imparts a local magnetic torque (i.e. the ability of the two-electron potential to locally rotate the magnetization with respect to a starting guess configuration). The inability of the two-electron potential to rotate the magnetization during the self-consistent treatment of SOC in the absence of Fock exchange results in different guesses for the orientation of the initial magnetization yielding different final solutions. On the other hand, with hybrid xc functionals, the same solution in terms of energy and spatial distribution of the magnetization can be consistently found, regardless of the starting guess.

The local magnetic torque due to the Fock operator improves the rotational invariance of the total energy in non-collinear GGA calculations.

Only the presence of the Fock exchange operator allows for the orbital- and spin-current densities (fundamental density variables of relativistic DFT) to properly evolve along the self-consistent treatment and to couple with the magnetization to yield physically meaningful solutions.

When space inversion symmetry is broken, the full breaking of the time-reversal symmetry in momentum space enabled by the presence of Fock exchange allows to explore certain electronic states that would otherwise be forbidden by a sum-rule which constrains the electronic band structure at opposite points in reciprocal space.

Appendix A: Working Expressions for the Density Matrix in Position Space

Substituting Eq. (21) in (22) and using Euler's formula, we find the following working expressions for the real and imaginary parts of the position space density matrix:

$$\begin{aligned}\Re[P^{\sigma\sigma'}_{\mu\nu\{\underline{\mathbf{g}}\}}] \;=\; & \frac{1}{\Omega_r}\int_{\Omega_r} d\underline{\mathbf{k}} \sum_i^{occ} \theta[\epsilon_F - \epsilon_{i\{\underline{\mathbf{k}}\}}]\Big\{ \cos(\underline{\mathbf{k}}\cdot\underline{\mathbf{g}}) \\ & \times \Big(\Re[c^{\sigma}_{\mu i\{\underline{\mathbf{k}}\}}]\Re[c^{\sigma'}_{\nu i\{\underline{\mathbf{k}}\}}] + \Im[c^{\sigma}_{\mu i\{\underline{\mathbf{k}}\}}]\Im[c^{\sigma'}_{\nu i\{\underline{\mathbf{k}}\}}]\Big) \\ & - \sin(\underline{\mathbf{k}}\cdot\underline{\mathbf{g}}) \\ & \times \Big(\Re[c^{\sigma}_{\mu i\{\underline{\mathbf{k}}\}}]\Im[c^{\sigma'}_{\nu i\{\underline{\mathbf{k}}\}}] - \Im[c^{\sigma}_{\mu i\{\underline{\mathbf{k}}\}}]\Re[c^{\sigma'}_{\nu i\{\underline{\mathbf{k}}\}}]\Big)\Big\},\end{aligned}$$

and:

$$\begin{aligned}\Im[P^{\sigma\sigma'}_{\mu\nu\{\underline{\mathbf{g}}\}}] \;=\; & \frac{1}{\Omega_r}\int_{\Omega_r} d\underline{\mathbf{k}} \sum_i^{occ} \theta[\epsilon_F - \epsilon_{i\{\underline{\mathbf{k}}\}}]\Big\{ \cos(\underline{\mathbf{k}}\cdot\underline{\mathbf{g}}) \\ & \times \Big(\Re[c^{\sigma}_{\mu i\{\underline{\mathbf{k}}\}}]\Im[c^{\sigma'}_{\nu i\{\underline{\mathbf{k}}\}}] - \Im[c^{\sigma}_{\mu i\{\underline{\mathbf{k}}\}}]\Re[c^{\sigma'}_{\nu i\{\underline{\mathbf{k}}\}}]\Big) \\ & + \sin(\underline{\mathbf{k}}\cdot\underline{\mathbf{g}}) \\ & \times \Big(\Re[c^{\sigma}_{\mu i\{\underline{\mathbf{k}}\}}]\Re[c^{\sigma'}_{\nu i\{\underline{\mathbf{k}}\}}] + \Im[c^{\sigma}_{\mu i\{\underline{\mathbf{k}}\}}]\Im[c^{\sigma'}_{\nu i\{\underline{\mathbf{k}}\}}]\Big)\Big\}.\end{aligned}$$

Appendix B: Dependence of the Orbital-Current Density on Blocks of the Density Matrix

We show here how the orbital-current density $\mathbf{j}(\mathbf{r})$ can be developped in terms of the single particle density matrix elements $P^{\sigma\sigma'}_{\mu\nu}$. To simplify the notation, the developments are provided for the non-periodic case, so that the subscripts $\{\mathbf{g}\}$ and $\{\mathbf{k}\}$ are dropped. The fact that we use the non-periodic limit, however does not change the conclusions on the functional dependence of $\mathbf{j}(\mathbf{r})$ on the density matrix. We also here drop the underlined notation for Cartesian vectors.

We therefore write the density matrix elements $P_{\mu\nu}^{\sigma\sigma'}$ in terms of the occupied orbital coefficients as follows:

$$P_{\mu\nu}^{\sigma\sigma'} = \sum_i \left[c_{\mu i}^{\sigma}\right]^* c_{\nu i}^{\sigma'} \,. \tag{B1}$$

The density matrix is complex-Hermitian:

$$P_{\mu\nu}^{\sigma\sigma'} = \left[P_{\nu\mu}^{\sigma'\sigma}\right]^* \,. \tag{B2}$$

In the non-periodic limit, we write the 2c spinors as in Eq. (2), but without the index $\mathbf{k}$:

$$\mathbf{\Psi}_i\left(\mathbf{r}\right) = \sum_\mu \left[c_{\mu i}^{\alpha}\boldsymbol{\alpha} + c_{\mu i}^{\beta}\boldsymbol{\beta}\right] \phi_\mu(\mathbf{r}) \,. \tag{B3}$$

The orbital-current density is written in terms of the occupied spinors $\mathbf{\Psi}_i\left(\mathbf{r}\right)$ as follows:

$$\mathbf{j}\left(\mathbf{r}\right) = \frac{1}{2i}\sum_i^{occ} \left[\mathbf{\Psi}_i\left(\mathbf{r}\right)\right]^\dagger \boldsymbol{\nabla}\mathbf{\Psi}_i\left(\mathbf{r}\right) - \left[\boldsymbol{\nabla}\mathbf{\Psi}_i\left(\mathbf{r}\right)\right]^\dagger \mathbf{\Psi}_i\left(\mathbf{r}\right) \,. \tag{B4}$$

Substituting Eq. (3), as well as Eq. (B3) in Eq. (B4):

$$\begin{aligned}\mathbf{j}\left(\mathbf{r}\right) &= \frac{1}{2i}\sum_i^{occ}\sum_{\mu\nu}\left(\left[c_{\mu i}^{\alpha}\right]^* c_{\nu i}^{\alpha} + \left[c_{\mu i}^{\beta}\right]^* c_{\nu i}^{\beta}\right) \\ &\times \left(\phi_\mu(\mathbf{r})\left[\boldsymbol{\nabla}\phi_\nu(\mathbf{r})\right] - \left[\boldsymbol{\nabla}\phi_\mu(\mathbf{r})\right]\phi_\nu(\mathbf{r})\right) \,.\end{aligned} \tag{B5}$$

Substituting Eq. (B1) in Eq. (B5), we obtain:

$$\begin{aligned}\mathbf{j}\left(\mathbf{r}\right) &= \frac{1}{2i}\sum_{\mu\nu}\left(P_{\mu\nu}^{\alpha\alpha} + P_{\mu\nu}^{\beta\beta}\right)\phi_\mu(\mathbf{r})\left[\boldsymbol{\nabla}\phi_\nu(\mathbf{r})\right] \\ &- \frac{1}{2i}\sum_{\mu\nu}\left(P_{\mu\nu}^{\alpha\alpha} + P_{\mu\nu}^{\beta\beta}\right)\left[\boldsymbol{\nabla}\phi_\mu(\mathbf{r})\right]\phi_\nu(\mathbf{r}) \,.\end{aligned} \tag{B6}$$

We can simplify each sum in Eq. (B6) using the Hermiticity of the density matrix from Eq. (B2), by writting, for example, for the first sum in Eq. (B6):

$$\begin{aligned}&\sum_{\mu\nu}\left(P_{\mu\nu}^{\alpha\alpha} + P_{\mu\nu}^{\beta\beta}\right)\phi_\mu(\mathbf{r})\left[\boldsymbol{\nabla}\phi_\nu(\mathbf{r})\right] = \frac{1}{2}\sum_{\mu\nu}\left(P_{\mu\nu}^{\alpha\alpha} + P_{\mu\nu}^{\beta\beta}\right) \\ &\times\phi_\mu(\mathbf{r})\left[\boldsymbol{\nabla}\phi_\nu(\mathbf{r})\right] + \frac{1}{2}\sum_{\mu\nu}\left(P_{\nu\mu}^{\alpha\alpha} + P_{\nu\mu}^{\beta\beta}\right)\left[\boldsymbol{\nabla}\phi_\mu(\mathbf{r})\right]\phi_\nu(\mathbf{r})\end{aligned} \tag{B7}$$

Substituting Eq. (B2) in Eq. (B7):

$$\begin{aligned}&\sum_{\mu\nu}\left(P_{\mu\nu}^{\alpha\alpha} + P_{\mu\nu}^{\beta\beta}\right)\phi_\mu(\mathbf{r})\left[\boldsymbol{\nabla}\phi_\nu(\mathbf{r})\right] = \\ &\frac{1}{2}\sum_{\mu\nu}\left(P_{\mu\nu}^{\alpha\alpha} + P_{\mu\nu}^{\beta\beta}\right)\phi_\mu(\mathbf{r})\left[\boldsymbol{\nabla}\phi_\nu(\mathbf{r})\right] \\ &+\frac{1}{2}\sum_{\mu\nu}\left(\left[P_{\mu\nu}^{\alpha\alpha}\right]^* + \left[P_{\mu\nu}^{\beta\beta}\right]^*\right)\left[\boldsymbol{\nabla}\phi_\mu(\mathbf{r})\right]\phi_\nu(\mathbf{r}) \,.\end{aligned} \tag{B8}$$

Proceeding similarly for the second sum in Eq. (B6), we obtain:

$$\begin{aligned}&\sum_{\mu\nu}\left(P_{\mu\nu}^{\alpha\alpha} + P_{\mu\nu}^{\beta\beta}\right)\left[\boldsymbol{\nabla}\phi_\mu(\mathbf{r})\right]\phi_\nu(\mathbf{r}) = \\ &\frac{1}{2}\sum_{\mu\nu}\left(P_{\mu\nu}^{\alpha\alpha} + P_{\mu\nu}^{\beta\beta}\right)\left[\boldsymbol{\nabla}\phi_\mu(\mathbf{r})\right]\phi_\nu(\mathbf{r}) \\ &+\frac{1}{2}\sum_{\mu\nu}\left(\left[P_{\mu\nu}^{\alpha\alpha}\right]^* + \left[P_{\mu\nu}^{\beta\beta}\right]^*\right)\phi_\mu(\mathbf{r})\left[\boldsymbol{\nabla}\phi_\nu(\mathbf{r})\right] \,.\end{aligned} \tag{B9}$$

Substituting Eqs. (B8) and (B9) in Eq. (B6), we find:

$$\begin{aligned}\mathbf{j}\left(\mathbf{r}\right) &= \frac{1}{4i}\sum_{\mu\nu}\left(P_{\mu\nu}^{\alpha\alpha} + P_{\mu\nu}^{\beta\beta}\right)\phi_\mu(\mathbf{r})\left[\boldsymbol{\nabla}\phi_\nu(\mathbf{r})\right] \\ &+ \frac{1}{4i}\sum_{\mu\nu}\left(\left[P_{\mu\nu}^{\alpha\alpha}\right]^* + \left[P_{\mu\nu}^{\beta\beta}\right]^*\right)\left[\boldsymbol{\nabla}\phi_\mu(\mathbf{r})\right]\phi_\nu(\mathbf{r}) \\ &- \frac{1}{4i}\sum_{\mu\nu}\left(P_{\mu\nu}^{\alpha\alpha} + P_{\mu\nu}^{\beta\beta}\right)\left[\boldsymbol{\nabla}\phi_\mu(\mathbf{r})\right]\phi_\nu(\mathbf{r}) \\ &- \frac{1}{4i}\sum_{\mu\nu}\left(\left[P_{\mu\nu}^{\alpha\alpha}\right]^* + \left[P_{\mu\nu}^{\beta\beta}\right]^*\right)\phi_\mu(\mathbf{r})\left[\boldsymbol{\nabla}\phi_\nu(\mathbf{r})\right]\end{aligned} \tag{B10}$$

Combining the first and fourth sums, as well as the second and third sums in Eq. (B10), we finally find:

$$\begin{aligned}\mathbf{j}\left(\mathbf{r}\right) &= \frac{1}{2}\sum_{\mu\nu}\left(\Im\left[P_{\mu\nu}^{\alpha\alpha}\right] + \Im\left[P_{\mu\nu}^{\beta\beta}\right]\right) \\ &\times \left\{\phi_\mu(\mathbf{r})\left[\boldsymbol{\nabla}\phi_\nu(\mathbf{r})\right] - \left[\boldsymbol{\nabla}\phi_\mu(\mathbf{r})\right]\phi_\nu(\mathbf{r})\right\} \,.\end{aligned} \tag{B11}$$

To write succinct expressions for the orbital-current density, as well as the other density variables in terms of the density matrix, it is useful to introduce the following compact notation:

$$P_{\mu\nu}^{\alpha\alpha\oplus\beta\beta} = P_{\mu\nu}^{\alpha\alpha} + P_{\mu\nu}^{\beta\beta} \tag{B12a}$$
$$P_{\mu\nu}^{\alpha\alpha\ominus\beta\beta} = P_{\mu\nu}^{\alpha\alpha} - P_{\mu\nu}^{\beta\beta} \tag{B12b}$$
$$P_{\mu\nu}^{\beta\alpha\oplus\alpha\beta} = P_{\mu\nu}^{\beta\alpha} + P_{\mu\nu}^{\alpha\beta} \tag{B12c}$$
$$P_{\mu\nu}^{\beta\alpha\ominus\alpha\beta} = P_{\mu\nu}^{\beta\alpha} - P_{\mu\nu}^{\alpha\beta} \,. \tag{B12d}$$

Using the notation in Eq. (B12a) we can write also the particle-number density and magnetization Cartesian components in terms of the density matrix as follows:[16,48]

$$n\left(\mathbf{r}\right) = \sum_{\mu\nu} \Re\left[P_{\mu\nu}^{\alpha\alpha\oplus\beta\beta}\right] \phi_\mu(\mathbf{r})\phi_\nu(\mathbf{r}) \tag{B13}$$

$$m_x\left(\mathbf{r}\right) = \sum_{\mu\nu} \Re\left[P_{\mu\nu}^{\beta\alpha\oplus\alpha\beta}\right] \phi_\mu(\mathbf{r})\phi_\nu(\mathbf{r}) \tag{B14}$$

$$m_y\left(\mathbf{r}\right) = -\sum_{\mu\nu} \Im\left[P_{\mu\nu}^{\beta\alpha\ominus\alpha\beta}\right] \phi_\mu(\mathbf{r})\phi_\nu(\mathbf{r}) \tag{B15}$$

$$m_z\left(\mathbf{r}\right) = \sum_{\mu\nu} \Re\left[P_{\mu\nu}^{\alpha\alpha\ominus\beta\beta}\right] \phi_\mu(\mathbf{r})\phi_\nu(\mathbf{r}) \,, \tag{B16}$$

and for the orbital-current density:

$$\mathbf{j}\left(\mathbf{r}\right) = \frac{1}{2}\sum_{\mu\nu}\Im\left[P_{\mu\nu}^{\alpha\alpha\oplus\beta\beta}\right]\Big\{\phi_{\mu}(\mathbf{r})\left[\boldsymbol{\nabla}\phi_{\nu}(\mathbf{r})\right] - \left[\boldsymbol{\nabla}\phi_{\mu}(\mathbf{r})\right]\phi_{\nu}(\mathbf{r})\Big\}\,. \tag{B17}$$

Comparing Eqs. (B13)-(B16) with Eq. (B17) we see that the n, $\mathbf{m}$ and $\mathbf{j}$ make use of all spin-blocks of the density matrix, except for the imaginary part of the $\beta\alpha\oplus\alpha\beta$ and $\alpha\alpha\ominus\beta\beta$ ones, as well as the real part of the $\beta\alpha\ominus\alpha\beta$ block. As we will see in Appendix C, these missing spin-blocks of the density matrix will be used to define the spin-current densities $\mathbf{J}_x$, $\mathbf{J}_y$ and $\mathbf{J}_z$.

Appendix C: Dependence of the Spin-Current Density on Blocks of the Density Matrix

We show here how the spin-current density $\mathbf{J}_c$ can be expressed in terms of the remaining spin-blocks of the density matrix. As in Appendix B, we adopt the non-periodic limit and drop the underlined notation for Cartesian vectors in order to simplify the notation.

For the spin-current density, the expression in terms of 2c spinors makes use of the 2×2 complex Pauli matrices:

$$\hat{\boldsymbol{\sigma}}_x = \begin{pmatrix}0 & 1\\ 1 & 0\end{pmatrix} \quad \hat{\boldsymbol{\sigma}}_y = \begin{pmatrix}0 & -i\\ i & 0\end{pmatrix} \quad \hat{\boldsymbol{\sigma}}_z = \begin{pmatrix}1 & 0\\ 0 & -1\end{pmatrix}\,, \tag{C1}$$

and reads as follows, in the non-periodic limit:

$$\mathbf{J}_c\left(\mathbf{r}\right) = \frac{1}{2i}\sum_{i}^{occ}\left[\boldsymbol{\Psi}_i\left(\mathbf{r}\right)\right]^{\dagger}\hat{\boldsymbol{\sigma}}_c\boldsymbol{\nabla}\boldsymbol{\Psi}_i\left(\mathbf{r}\right) - \left[\boldsymbol{\nabla}\boldsymbol{\Psi}_i\left(\mathbf{r}\right)\right]^{\dagger}\hat{\boldsymbol{\sigma}}_c\boldsymbol{\Psi}_i\left(\mathbf{r}\right)\,, \tag{C2}$$

where $c = x, y, z$ is a Cartesian index labelling the Pauli matrices. Substituting Eqs. (B3) and (C1) in Eq. (C2) and proceeding as in Eqs. (B5) and (B6), we find the following expressions for all three components:

$$\mathbf{J}_x\left(\mathbf{r}\right) = \frac{1}{2i}\sum_{\mu\nu}\left(P_{\mu\nu}^{\alpha\beta} + P_{\mu\nu}^{\beta\alpha}\right) \times \Big\{\phi_{\mu}(\mathbf{r})\left[\boldsymbol{\nabla}\phi_{\nu}(\mathbf{r})\right] - \left[\boldsymbol{\nabla}\phi_{\mu}(\mathbf{r})\right]\phi_{\nu}(\mathbf{r})\Big\} \tag{C3a}$$

$$\mathbf{J}_y\left(\mathbf{r}\right) = \frac{1}{2}\sum_{\mu\nu}\left(P_{\mu\nu}^{\beta\alpha} - P_{\mu\nu}^{\alpha\beta}\right) \times \Big\{\phi_{\mu}(\mathbf{r})\left[\boldsymbol{\nabla}\phi_{\nu}(\mathbf{r})\right] - \left[\boldsymbol{\nabla}\phi_{\mu}(\mathbf{r})\right]\phi_{\nu}(\mathbf{r})\Big\} \tag{C3b}$$

$$\mathbf{J}_z\left(\mathbf{r}\right) = \frac{1}{2i}\sum_{\mu\nu}\left(P_{\mu\nu}^{\alpha\alpha} - P_{\mu\nu}^{\beta\beta}\right) \times \Big\{\phi_{\mu}(\mathbf{r})\left[\boldsymbol{\nabla}\phi_{\nu}(\mathbf{r})\right] - \left[\boldsymbol{\nabla}\phi_{\mu}(\mathbf{r})\right]\phi_{\nu}(\mathbf{r})\Big\} \tag{C3c}$$

Then, proceeding as in Eqs. (B7)-(B10), we find the following expressions:

$$\mathbf{J}_x\left(\mathbf{r}\right) = \frac{1}{4i}\sum_{\mu\nu}\left(P_{\mu\nu}^{\alpha\beta} - \left[P_{\mu\nu}^{\alpha\beta}\right]^{*} + P_{\mu\nu}^{\beta\alpha} - \left[P_{\mu\nu}^{\beta\alpha}\right]^{*}\right) \times \Big\{\phi_{\mu}(\mathbf{r})\left[\boldsymbol{\nabla}\phi_{\nu}(\mathbf{r})\right] - \left[\boldsymbol{\nabla}\phi_{\mu}(\mathbf{r})\right]\phi_{\nu}(\mathbf{r})\Big\}\,, \tag{C4a}$$

$$\mathbf{J}_y\left(\mathbf{r}\right) = \frac{1}{4}\sum_{\mu\nu}\left(P_{\mu\nu}^{\beta\alpha} + \left[P_{\mu\nu}^{\beta\alpha}\right]^{*} - P_{\mu\nu}^{\alpha\beta} - \left[P_{\mu\nu}^{\alpha\beta}\right]^{*}\right) \times \Big\{\phi_{\mu}(\mathbf{r})\left[\boldsymbol{\nabla}\phi_{\nu}(\mathbf{r})\right] - \left[\boldsymbol{\nabla}\phi_{\mu}(\mathbf{r})\right]\phi_{\nu}(\mathbf{r})\Big\}\,, \tag{C4b}$$

$$\mathbf{J}_z\left(\mathbf{r}\right) = \frac{1}{4i}\sum_{\mu\nu}\left(P_{\mu\nu}^{\alpha\alpha} - \left[P_{\mu\nu}^{\alpha\alpha}\right]^{*} - P_{\mu\nu}^{\beta\beta} + \left[P_{\mu\nu}^{\beta\beta}\right]^{*}\right) \times \Big\{\phi_{\mu}(\mathbf{r})\left[\boldsymbol{\nabla}\phi_{\nu}(\mathbf{r})\right] - \left[\boldsymbol{\nabla}\phi_{\mu}(\mathbf{r})\right]\phi_{\nu}(\mathbf{r})\Big\}\,. \tag{C4c}$$

Finally, using again the Hermiticity of the density matrix by substituting Eq. (B2) in Eq. (C5), we obtain:

$$\mathbf{J}_x\left(\mathbf{r}\right) = \frac{1}{2}\sum_{\mu\nu}\Im\left[P_{\mu\nu}^{\beta\alpha\oplus\alpha\beta}\right]\Big\{\phi_{\mu}(\mathbf{r})\left[\boldsymbol{\nabla}\phi_{\nu}(\mathbf{r})\right] - \left[\boldsymbol{\nabla}\phi_{\mu}(\mathbf{r})\right]\phi_{\nu}(\mathbf{r})\Big\}\,, \tag{C5a}$$

$$\mathbf{J}_y\left(\mathbf{r}\right) = \frac{1}{2}\sum_{\mu\nu}\Re\left[P_{\mu\nu}^{\beta\alpha\ominus\alpha\beta}\right]\Big\{\phi_{\mu}(\mathbf{r})\left[\boldsymbol{\nabla}\phi_{\nu}(\mathbf{r})\right] - \left[\boldsymbol{\nabla}\phi_{\mu}(\mathbf{r})\right]\phi_{\nu}(\mathbf{r})\Big\}\,, \tag{C5b}$$

$$\mathbf{J}_z\left(\mathbf{r}\right) = \frac{1}{2}\sum_{\mu\nu}\Im\left[P_{\mu\nu}^{\alpha\alpha\ominus\beta\beta}\right]\Big\{\phi_{\mu}(\mathbf{r})\left[\boldsymbol{\nabla}\phi_{\nu}(\mathbf{r})\right] - \left[\boldsymbol{\nabla}\phi_{\mu}(\mathbf{r})\right]\phi_{\nu}(\mathbf{r})\Big\}\,. \tag{C5c}$$

* Electronic address: jkd788@mail.usask.ca
† Electronic address: alessandro.erba@unito.it

[1] S. Tomita, H. Kurosawa, T. Ueda, and K. Sawada, J. Phys. D: Appl. Phys. **51**, 083001 (2018).
[2] S. Grytsiuk, M. Hoffmann, J.-P. Hanke, P. Mavropoulos, Y. Mokrousov, G. Bihlmayer, and S. Blügel, Phys. Rev. B **100**, 214406 (2019).
[3] G. Vignale, J. Supercond. Nov. Magn. **23**, 3 (2010).
[4] D. Bercioux and P. Lucignano, Rep. Prog. Phys. **78**, 106001 (2015).
[5] G. Dresselhaus, Phys. Rev. **100**, 580 (1955).
[6] E. I. Rashba, Soviet Phys. Solid State **2**, 1109 (1960).
[7] X. Wang, A. Qaiumzadeh, and A. Brataas, Phys. Rev. Lett. **123**, 147203 (2019).
[8] J. E. Moore, Nature **464**, 194 (2010).
[9] K. G. Dyall and K. Faegri, *Introduction to relativistic quantum chemistry* (Oxford University Press, 2007).
[10] M. Reiher and A. Wolf, *Relativistic quantum chemistry: the fundamental theory of molecular science* (John Wiley & Sons, 2014).
[11] L. Z. W. Zhu and S. Trickey, J. Chem. Phys. **145**, 224106 (2016).
[12] E. Engel, *Relativistic density functional theory: foundations and basic formalism in Theor. Comput. Chem.*, vol. 11 (Elsevier, 2002).
[13] C. van Wüllen, *Relativistic density functional calculations on small molecules in Theor. Comput. Chem.*, vol. 14 (Elsevier, 2004).
[14] C. R. Jacob and M. Reiher, Int. J. Quantum Chem. **112**, 3661 (2012).
[15] A. E. Mattsson and J. M. Wills, Int. J. Quantum Chem. **116**, 834 (2016).
[16] J. K. Desmarais, J.-P. Flament, and A. Erba, J. Chem. Phys. **151**, 074108 (2019).
[17] J. K. Desmarais, J.-P. Flament, and A. Erba, J. Phys. Chem. Lett. **10**, 3580 (2019).
[18] Z. Zhang, Theor. Chem. Acc. **133**, 1588 (2014).
[19] M. K. Armbruster, F. Weigend, C. van Wüllen, and W. Klopper, Phys. Chem. Chem. Phys. **10**, 1748 (2008).
[20] J. Kubler, K.-H. Hock, J. Sticht, and A. Williams, J. Phys. F **18**, 469 (1988).
[21] I. W. Bulik, G. Scalmani, M. J. Frisch, and G. E. Scuseria, Phys. Rev. B **87**, 035117 (2013).
[22] J. E. Peralta, G. E. Scuseria, and M. J. Frisch, Phys. Rev. B **75**, 125119 (2007).
[23] D. Hobbs, G. Kresse, and J. Hafner, Phys. Rev. B **62**, 11556 (2000).
[24] G. Scalmani and M. J. Frisch, J. Chem. Theor. Comput. **8**, 2193 (2012).
[25] K. Knöpfle, L. Sandratskii, and J. Kübler, Phys. Rev. B **62**, 5564 (2000).
[26] V. García-Suárez, C. Newman, C. J. Lambert, J. Pruneda, and J. Ferrer, Eur. Phys. J. B **40**, 371 (2004).
[27] P. Kurz, F. Förster, L. Nordström, G. Bihlmayer, and S. Blügel, Phys. Rev. B **69**, 024415 (2004).
[28] A. Dal Corso and A. M. Conte, Phys. Rev. B **71**, 115106 (2005).
[29] U. von Barth and L. Hedin, J. Phys. C **5**, 1629 (1972).
[30] S. Sharma, E. K. U. Gross, A. Sanna, and J. K. Dewhurst, J. Chem. Theo. Comput. **14**, 1247 (2018).
[31] G. Vignale and M. Rasolt, Phys. Rev. B **37**, 10685 (1988).
[32] K. Bencheikh, J. of Phys. A **36**, 11929 (2003).
[33] A. Becke, Cad. J. Chem. **74**, 995 (1996).
[34] A. Becke, J. Chem. Phys. **117**, 6935 (2002).
[35] E. R. Johnson, R. M. Dickson, and A. D. Becke, J. Chem. Phys. **126**, 184104 (2007).
[36] S. N. Maximoff, M. Ernzerhof, and G. E. Scuseria, J. Chem. Phys. **120**, 2105 (2004).
[37] E. R. S. Pittalis and E. Gross, Phys. Rev. A **80**, 032515 (2009).
[38] S. Pittalis, S. Kurth, S. Sharma, and E. Gross, J. Chem. Phys. **127**, 124103 (2007).
[39] E. R. S. Pittalis and C. Proetto, Phys. Rev. B **81**, 115108 (2010).
[40] S. P. E. Räsänen and C. Proetto, J. Chem. Phys. **132**, 044112 (2010).
[41] J. J. Tao and J. Perdew, Phys. Rev. Lett. **95**, 196403 (2005).
[42] F. Egidi, S. Sun, J. J. Goings, G. Scalmani, M. J. Frisch, and X. Li, J. Chem. Theor. Comput. **13**, 2591 (2017).
[43] P. C. S. Komorovsky and M. Repisky, J. Chem. Phys. **151**, 184111 (2019).
[44] F. Eich and E. Gross, Physical review letters **111**, 156401 (2013).
[45] F. Eich, S. Pittalis, and G. Vignale, Physical Review B **88**, 245102 (2013).
[46] S. Pittalis, G. Vignale, and F. Eich, Phys. Rev. B **96**, 035141 (2017).
[47] J. Anton, B. Fricke, and P. Schwerdtfeger, Chem. Phys. **311**, 97 (2005).
[48] J. K. Desmarais, J.-P. Flament, and A. Erba, J. Chem. Phys. **151**, 074107 (2019).
[49] K. Capelle, G. Vignale, and B. Györffy, Phys. Rev. Lett. **87**, 206403 (2001).
[50] S. Sharma, J. Dewhurst, C. Ambrosch-Draxl, S. Kurth, N. Helbig, S. Pittalis, S. Shallcross, L. Nordström, and E. Gross, Phys. Rev. Lett. **98**, 196405 (2007).
[51] S. Sharma, S. Pittalis, S. Kurth, S. Shallcross, J. Dewhurst, and E. Gross, Phys. Rev. B **76**, 100401 (2007).
[52] D. Koelling and B. Harmon, J. Phys. C **10**, 3107 (1977).
[53] H. J. C. Li, A.J. Freeman and C. Fu, Phys. Rev. B **42**, 5433 (1990).
[54] M. M. S. Steiner, S. Khmelevskyi and G. Kresse, Phys. Rev. B **93**, 224425 (2016).
[55] Http://elk.sourceforge.net/.
[56] A. Gulans, S. Kontur, C. Meisenbichler, D. Nabok, P. Pavone, S. Rigamonti, S. Sagmeister, U. Werner, and C. Draxl, J. Phys. Condens. Matt. **26**, 363202 (2014).
[57] Http://www.flapw.de/.
[58] E. Trushin and A. Görling, Phys. Rev. B **98**, 205137 (2018).
[59] R. Dovesi, A. Erba, R. Orlando, C. M. Zicovich-Wilson, B. Civalleri, L. Maschio, M. Rérat, S. Casassa, J. Baima, S. Salustro, et al., WIREs Comput. Mol. Sci. **8**, e1360 (2018).
[60] J. Desmarais, A. Erba, and R. Dovesi, Theor. Chem. Acc. **137**, 28 (2018).
[61] X. Cao and M. Dolg, Coor. Chem. Rev. **250**, 900 (2006).
[62] Y. S. Lee, W. C. Ermler, and K. S. Pitzer, in *Molecular Structure And Statistical Thermodynamics: Selected Papers of Kenneth S Pitzer* (World Scientific, 1993), pp. 112–127.

[63] C. Pisani, R. Dovesi, and C. Roetti, in *Hartree—Fock ab initio treatment of crystalline systems* (1988), vol. 48.
[64] B. W. Roberts, Philosophy of Science **84**, 315 (2017).
[65] See Supplemental Material at URL for the derivation of Eq. (29) of the main body of the manuscript.
[66] K. Capelle and E. K. U. Gross, Phys. Rev. Lett. **78**, 1872 (1997).
[67] A. Petrone, D. B. Williams-Young, S. Sun, T. F. Stetina, and X. Li, Eur. Phys. J. B **91**, 169 (2018).
[68] A. Erba, J. Baima, I. Bush, R. Orlando, and R. Dovesi, J. Chem. Theory Comput. **13**, 5019 (2017).
[69] R. Dovesi, C. Ermondi, E. Ferrero, C. Pisani, and C. Roetti, Physical Review B **29**, 3591 (1984).
[70] H. Stoll, B. Metz, and M. Dolg, J. Comput. Chem. **23**, 767 (2002).
[71] P. A. Dirac, in *Math. Proc. Camb. Philo. Soc.* (Cambridge University Press, 1930), vol. 26, pp. 376–385.
[72] S. H. Vosko, L. Wilk, and M. Nusair, Can. J. Phys. **58**, 1200 (1980).
[73] J. P. Perdew, K. Burke, and M. Ernzerhof, Phys. Rev. Lett. **77**, 3865 (1996).
[74] G. Karlström, Chem. Phys. Lett. **67**, 348 (1979).
[75] E. Cancès and C. Le Bris, Int. J. Quantum Chem. **79**, 82 (2000).
[76] K. N. Kudin, G. E. Scuseria, and E. Cances, J. Chem. Phys. **116**, 8255 (2002).
[77] M. D. Towler, A. Zupan, and M. Causà, Comput. Phys. Comm. **98**, 181 (1996).
[78] V. I. Lebedev, USSR Comput. Math. Math. Phys. **16**, 10 (1976).
[79] V. I. Lebedev, Siber. Math. J. **18**, 99 (1977).
[80] A. D. Becke, J. Chem. Phys. **88**, 1053 (1988).
[81] R. Dovesi, V. Saunders, C. Roetti, R. Orlando, C. Zicovich-Wilson, F. Pascale, B. Civalleri, K. Doll, N. Harrison, I. Bush, et al., *CRYSTAL17 User's Manual*, Università di Torino, Torino (2017), http://www.crystal.unito.it.
[82] C. Adamo and V. Barone, J. Chem. Phys. **110**, 6158 (1999).
[83] A. D. Becke, J. Chem. Phys. **98**, 1372 (1993).